Synthesis, pharmacological and structural studies of 5-substituted-3-(1-arylmethyl-1,2,3,6-tetrahydropyridin-4-yl)-1*H*-indoles as multi-target ligands of aminergic GPCRs

Magda Kondej[1], Tomasz M. Wróbel[1,2], Andrea G. Silva[3], Piotr Stępnicki[1], Oliwia Koszła[1], Ewa Kędzierska[4], Agata Bartyzel[5], Grażyna Biała[4], Dariusz Matosiuk[1], Maria I. Loza[3], Marián Castro[3], Agnieszka A. Kaczor[1,6*]

[1]*Department of Synthesis and Chemical Technology of Pharmaceutical Substances, Faculty of Pharmacy with Division of Medical Analytics, Medical University of Lublin, 4A Chodźki St., PL-20093 Lublin, Poland*

[2]*Department of Drug Design and Pharmacology, Faculty of Health and Medical Sciences, University of Copenhagen, Universitetsparken 2, 2100 Copenhagen, Denmark*

[3]*Department of Pharmacology, Universidade de Santiago de Compostela, Center for Research in Molecular Medicine and Chronic Diseases (CIMUS), Avda de Barcelona, E-15782 Santiago de Compostela, Spain*

[4]*Department of Pharmacology and Pharmacodynamics, Faculty of Pharmacy with Division of Medical Analytics, Medical University of Lublin, 4A Chodźki St., PL-20093 Lublin, Poland*

[5]*Department of General and Coordination Chemistry, Maria Curie-Skłodowska University, M. Curie-Skłodowskiej Sq. 2, PL-20031 Lublin, Poland*

[6]*School of Pharmacy, University of Eastern Finland, Yliopistonranta 1, P.O. Box 1627, FI-70211 Kuopio, Finland*

E-mail: agnieszka.kaczor@umlub.pl

Abstract: Schizophrenia is a complex disease with not fully understood pathomechanism, involving many neurotransmitters and their receptors. This is why it is best treated with multi-target drugs, such as second generation antipsychotics. Here we present 5-substituted-3-(1-arylmethyl-1,2,3,6-tetrahydropyridin-4-yl)-1*H*-indoles (**1**-**20**) which are ligands of dopamine D_2 and serotonin 5-HT_{1A} and 5-HT_{2A} receptors and display affinity in the nanomolar range. These compounds were designed as modifications of the virtual hit experimentally confirmed, D2AAK1, and synthesized from indole or 5-alkoxyindoles and *N*-substituted piperidin-4-ones in methanol in the presence of potassium hydroxide. Compound **9** was subjected to X-ray studies and it crystallizes in the centrosymmetric monoclinic space group $P2_1/c$ with one molecule in an asymmetric unit. Three most potent compounds (**5**, **9** and **17**) turned out to be antagonists of both D_2 and 5-HT_{2A} receptors what is beneficial for their potential application as antipsychotics. Compound **5** was subjected to behavioral studies and exhibited antipsychotic, pro-cognitive and antidepressant activity in appropriate mice models. Structure-activity relationships for compounds **1**-**20** were rationalized using molecular docking. It was found that, in general, bulky C5-alkoxy substituents at the indole moiety are not favorable as they direct towards aqueous environment of the extracellular vestibule. **Keywords:** antipsychotics; behavioral studies, G protein-coupled receptors; indole derivatives; multi-target compounds; schizophrenia.

Graphical abstract:

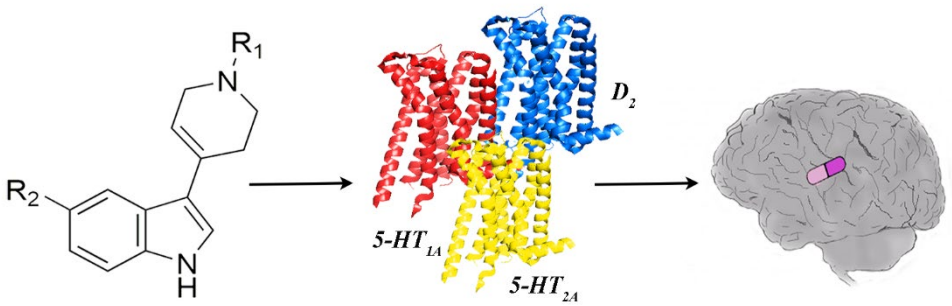

Highlights:

- Novel multi-target ligands of aminergic GPCRs.
- Antagonists of dopamine D_2 and serotonin 5-HT_{2A} receptors.
- Compound **5** exhibits antipsychotic, pro-cognitive and antidepressant activity.
- X-ray studies of compound **9** reveal energetically stable conformation.
- Molecular docking enables to rationalize the observed SAR.

1. Introduction

For a long time, the classical strategy of a drug action, consisting in one molecule targeting one certain receptor, was in the lead of the pharmacological approaches to the treatment of central nervous system diseases. This "magic bullet" paradigm was thought to be superior to multi-target "magic shotgun" concept, which assumes several molecular targets being simultaneously modulated by one molecule of a drug. The advantage of selectively acting drugs was based on the assumption that there is lower possibility to cause adverse effects comparing to drugs acting via a number of receptors. However, the complexity of central nervous system diseases often constitutes an obstacle to effective treatment with selective drugs. Therefore, the currently predominant approach in drug discovery is to search for one molecule that would be able to affect several targets [1]. Multi-target agents exert their effect through a wide range of receptors and involve several neurotransmitter pathways, what may be beneficial to the treatment of such diseases, since they are usually associated with impairment in transmission of more than one neuronal messenger. Moreover, applying one multi-target drug instead of a few selective drugs may reduce the frequency of side effects occurrence and allows to avoid drug-drug interactions [2].

One of the central nervous system diseases characterized by complex pathomechanism, involving a number of neurotransmitters, is schizophrenia. Ranking as the 15th top leading cause of disability among the population worldwide [3], schizophrenia has a major impact in health care systems and society. It is estimated that the disease affects 1% of global population with its beginning observed usually in early adulthood [4]. This chronic, severe mental disorder is characterized by dysfunctions in perception, thought processes and behavior, as well as cognitive and memory impairment. Patients suffering from schizophrenia experience symptoms such as hallucinations, delusions, disorganized speech or movement disorders, anhedonia, flattening or social withdrawal [5].

The etiology of schizophrenia involves environmental and genetic components, which may constitute predisposing factors for the development of the disease. Nonetheless, the exact causes of schizophrenia are still not satisfactorily understood. The main concept explaining the basis of the disease is related to dysfunctions in dopaminergic transmission in the mesolimbic pathway, resulting in positive symptoms, and in the mesocortical circuit, associated with the occurrence of negative symptoms. Schizophrenia is treated with antipsychotic drugs that fall into three generations. Classical first generation drugs are dopamine D_2 receptor antagonists and are effective against positive symptoms, with low affinity to reduce negative symptoms. Newer antipsychotics possess multi-target profile of action since they exhibit additional affinity for other molecular targets, and notably for serotonin receptors. Drugs of second generation bind to serotonin 5-HT_{2A} receptor with higher affinity than to D_2 receptor. Affecting serotonin neurotransmission may be beneficial to the pharmacotherapy of schizophrenic patients. Activation of 5-HT_{1A} receptor leads to increased release of dopamine in the mesocortical circuit, what may contribute to enhancing efficacy against negative and cognitive symptoms [6]. Antagonism at serotonin 5-HT_{2A} receptors, which are located on dopaminergic neurons, results in reducing negative symptoms of schizophrenia and improving extrapyramidal side effects profile of atypical antipsychotics, due to increased activity of nigrostriatal dopaminergic circuit [7]. Thus, multi-target drugs for the treatment of schizophrenia are more potent agents with a wider range of symptoms that are alleviated and with a safer profile.

In previous studies, we performed structure-based virtual screening in order to identify novel antagonists of dopamine D_2 receptor with potential application in the treatment of schizophrenia [8]. As a result, D2AAK1 (Fig. 1) with K_i of 58 nM to D_2 receptor has been found. This compound is characterized by multi-target profile, since it possesses additional affinity to D_1, D_3, 5-HT_{1A} and 5-HT_{2A} receptors (K_i of 1418, 614, 125 and 358 nM, respectively). Functional studies confirmed that D2AAK1 is an antagonist of D_2 and 5-HT_{2A}

receptor and partial agonist of 5-HT_{1A} receptor, what is beneficial for antipsychotic activity. Subsequent behavioral studies of D2AAK1 confirmed its antipsychotic properties, evaluated in a classical test consisting in reducing amphetamine-induced hyperactivity in mice. Moreover, the studied compound exerts anxiolytic and pro-cognitive effect *in vivo* [9].

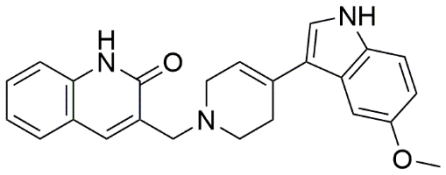

D2AAK1

Fig. 1. Structure of virtual hit, D2AAK1.

In this work, as a continuation of the raised subject, we aimed at finding novel potential antipsychotics with multi-target receptor profile, what has been achieved by designing and synthesizing analogues of the lead structure D2AAK1. Performed modifications include replacement of the substituent attached to nitrogen atom of 1,2,3,6-tetrahydropyridin-4-yl moiety and removing methoxy group from position 5 of the indole moiety or implementing ethoxy or isopropoxy group in this position.. Due to the promising activity of D2AAK1 and the presence of a protonatable nitrogen atom that is crucial for interactions with aminergic GPCRs, we decided to keep 3-(1,2,3,6-tetrahydropyridin-4-yl)-1*H*-indole scaffold, a new set-up with potential antipsychotic activity. The obtained compounds were then subjected to molecular modeling, X-ray, and detailed *in vitro* and behavioral studies to characterize their pharmacological multitarget profile and activity as potential antipsychotics.

2. Results

2.1. Chemistry

For the synthesis of compounds **1**-**20** we adopted the method developed by Guillaume et al. [10]. Shortly, indole or 5-alkoxyindole was heated with a variety of commercially available *N*-substituted piperidin-4-ones in 1M potassium hydroxide methanol solution at 75 °C in a sealed vial (Scheme 1). This straightforward method proved to be superior in our hands to

the reaction under acidic conditions [11] and allowed for the rapid synthesis of the desired compounds with minimal efforts invested in purification. Synthesis of compound **11**, under slightly different conditions was described by us before [13]. Precise structures of obtained compounds are presented in Table 2.

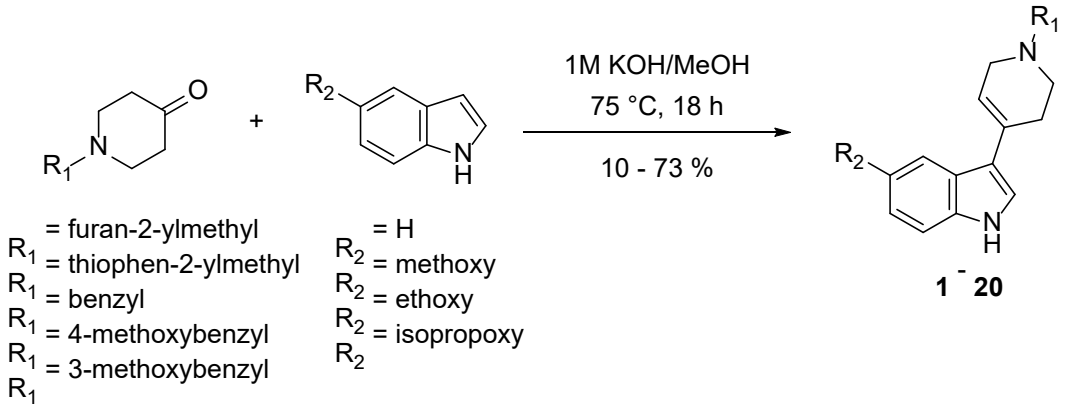

Scheme 1. Synthesis of compounds **1**-**20**.

2.2. X-ray studies

The molecular structure of 3-(1-benzyl-1,2,3,6-tetrahydropyridin-4-yl)-1*H*-indole (**9**), including the atom labelling, is shown in Fig. 2. Compound crystallizes in the centrosymmetric monoclinic space group $P2_1/c$ with one molecule in an asymmetric unit. The interatomic distances and angles agree with those described in the literature [12] and are comparable with those observed for other closely related indole derivatives [13–16]. However, there is a fluctuation of bond distances involving carbon atoms in benzene. The bond length C(17)-C(18) is slightly lower (1.333(5) Å) than that observed for C_{ar}⋯C_{ar} bonds (~1.380 Å). The indole ring of the compound is planar with a maximum deviation of 0.019(2) Å of (C8) atom from the best plane. The tetrahydropyridine ring is slightly inclined to the indole ring system by 14.6(1)°. The r.m.s. atomic displacement for the nonhydrogen atoms in indole ring-tetrahydropyridine moiety is 0.188(2) Å. The mean plane of the remaining part of compound i.e. the phenyl ring ((C15)–(C20)) is nearly perpendicular to the plane created by the rest of the molecule, forming an angle of 86.79(6)°. Similar to the previously described indole derivative (3-(1-benzyl-1,2,3,6-

tetrahydropyridin-4-yl)-5-ethoxy-1*H*-indole, (**11**) [13] the tetrahydropyridine ring system adopts a half-chair conformation [17–20]. In contrast to compound **11**, the N2 atom in compound **9** is below (-0.339(1) Å) and C5 atom lies above (0.320(1) Å) the mean plane defined by non-hydrogen N2/C13/C12/C11/C10/C9 atoms (the puckering parameters: Q = 0.506(1) Å, θ = 50.6(1)° and φ = 333.8(1)°)

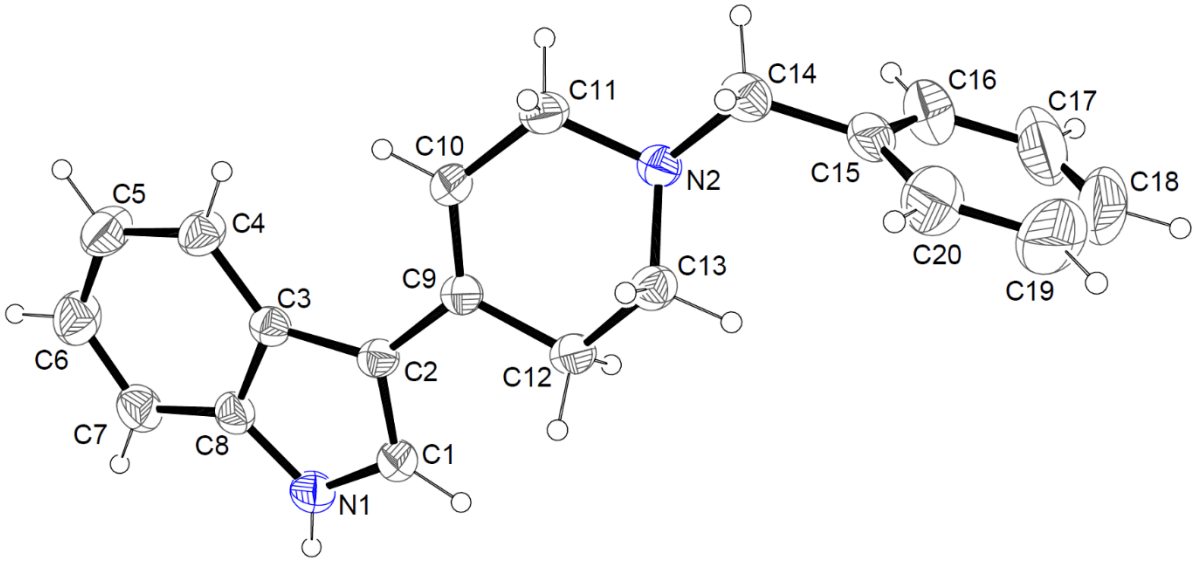

Fig. 2. A view of the molecular structure of **9**, with the atom labeling and displacement ellipsoids drawn at the 30% probability level.

The difference in conformation between **9** and **11** is shown in Fig. 3.

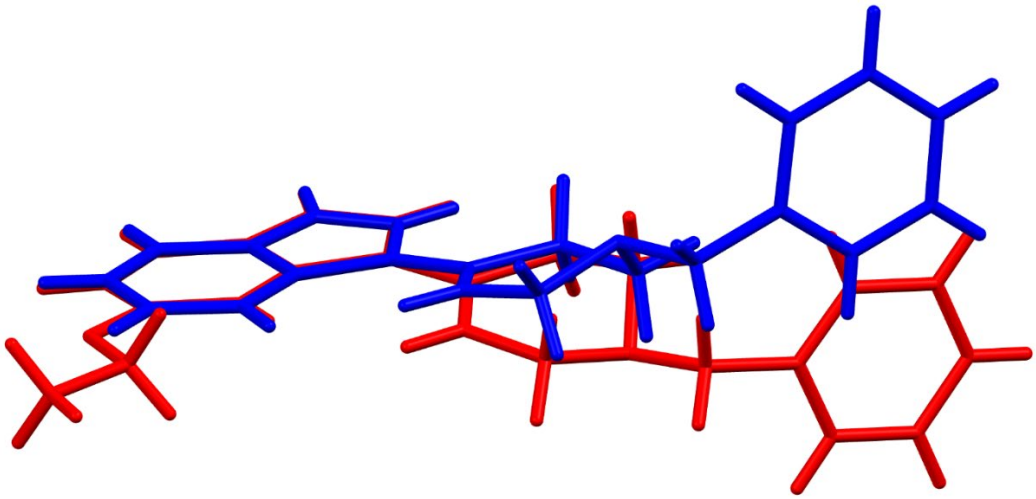

Fig. 3. Comparison between the structure of **9** (blue) and **11** (red).

The crystal packing of compound **9** was determined by intermolecular hydrogen bonds of the N–H···N type (Table 1). The hydrogen bonds between the indole and tetrahydropyridine rings of neighboring molecules form a one-dimensional network with a C(8) infinite chain motif [21] (see Supplementary Information, Fig. S1). As a result, the molecules are ordered into infinite ribbons extending along the [010] direction (Figs. S1B and S2).

Table 1. Hydrogen bonding and C-H···*Cg* interactions geometry of compound **9**.

Hydrogen bond [Å, º]				
D-H···A	**d(D-H)**	**d(H···A)**	**d(D···A)**	**∠ DHA**
N(1)–H(1N)···N(2)^{i}	0.84(2)	2.40(2).	3.195(2)	158(2)
C-H···Cg interactions [Å, º]				
C-H ···*Cg*	**d(D-H)**	**d(H···Cg)**	**d(C···Cg)**	**∠ CH*Cg***
C(12)–H(12A)···*Cg*(1)^{i}	0.97	3.00	3.621(2)	123
C(12)–H(12A)···*Cg*(3)^{i}	0.97	2.92	3.789(2)	149

Symmetry codes: (i) -x,y+1/2,-z+1/2; *Cg*1 and *Cg*3 are the centroids of the N1/C1/C2/C3/C8 and C3/C4/C5/C6/C7/C8 rings, respectively.

2.3. Affinity of compounds at selected targets

The affinity of the compounds for dopamine D_2, and serotonin 5-HT_{1A} and 5-HT_{2A} receptors was evaluated in *in vitro* radioligand binding assays, on cell membranes from cell lines stably expressing the cloned human receptors. Compounds were evaluated at a single (10 μM) concentration and for those showing an inhibition of the specific radioligand binding (%inh.) higher than 65%, concentration-response curves were constructed in order to determine their dissociation constant (K_i). This resulted in 18 compounds evaluated in concentration-response curves at D_2, the 20 compounds evaluated at 5-HT_{1A} receptors, and 6 compounds evaluated at 5-HT_{2A} receptors. Affinity (pK_i, K_i) values or %inh. at 10 μM are given in Table 2. Unless otherwise indicated, compounds for which K_i values are given fully displaced the specific radioligand binding at the highest concentrations assayed (either 10 μM or 100 μM)

(Supplementary Figures S3, S4 and S5 for D_2, 5-HT_{1A} and 5-HT_{2A} binding assays, respectively). Five compounds (compounds **5**, **9**, **10**, **13** and **17**) displayed affinities at D_2 receptors within the low to moderate nanomolar range, three of them (compounds **5**, **9** and **17**) showing multitarget affinity profiles in the nanomolar range at 5-HT_{1A} and 5-HT_{2A} receptors.

Table 2. Competitive radioligand binding data at human D_2, 5-HT_{1A} and 5-HT_{2A} receptors.

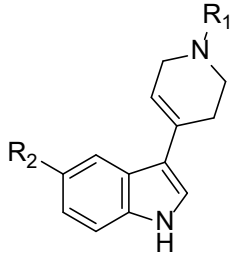

Compound	R_1	R_2	D_2	5-HT_{1A}	5-HT_{2A}
D2AAK1	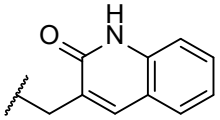	OMe	58 [8]	125 [8]	358 [8]
1	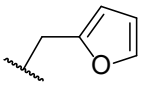	H	257 ± 60	752 ± 6	173 ± 1
2		OMe	142 ± 18[a]	195 ± 33	15 ± 1%
3		OEt	62 ± 1%	486 ± 118	47 ± 7%
4		OiPr	51 ± 1%	431 ± 55	5 ± 10%
5	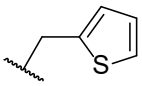	H	72 ± 23.1	305 ± 11	171 ± 28
6		OMe	141 ± 33	157 ± 13	1888 ± 373
7		OEt	166 ± 66[a]	139 ± 33	0 ± 2%
8		OiPr	465 ± 165	214 ± 1	14 ± 2%
9	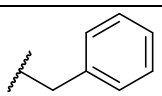	H	26 ± 9.9	354 ± 45	125 ± 35

10		OMe	63 ± 16.6	139 ± 27	41 ± 10%
11		OEt	151 ± 17 [13]	220 ± 45	2099 ± 745[a]
12		OiPr	321 ± 60	203 ± 11	32 ± 12%
13	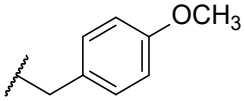	H	87 ± 11.1	243 ± 31	52 ± 6%
14		OMe	148 ± 26	134 ± 7	48 ± 1%
15		OEt	132 ± 35	194 ± 56	38 ± 3%
16		OiPr	165 ± 28	378 ± 76	36 ± 1%
17	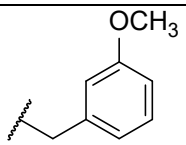	H	27 ± 10.1	243 ± 17	194 ± 34
18		OMe	112 ± 15	135 ± 19	24 ± 6%
19		OEt	108 ± 25	160 ± 9	3 ± 3%
20		OiPr	299 ± 68	290 ± 80	43 ± 8%
Haloperidol			3.25 ± 0.18		
5-Carboxamidotryptamine				0.34 ± 0.02	
Risperidone					0.37 ± 0.09

Data are expressed as %inh. at 10 μM (mean ± SEM of 1 -3 experiments performed in duplicate) or K_i (nM) (mean ± SEM of 2 - 3 independent experiments performed in duplicate) when full displacement was achieved. [a]Full displacement of specific binding was not achieved at the maximum concentration assayed (100 μM) so K_i value retrieved from the analysis might be not accurate.

2.4. Structure-activity relationships

Compounds with C5 unsubstituted indole generally displayed enhanced affinity towards D_2 receptor. As the bulkiness of R_2 alkoxy fragment increased the affinity dropped. Size of the R_1 substituent attached to the tetrahydropyridine fragment seemed to have less pronounced effect. Compounds with benzyl (**9**) and 3-methoxybenzyl (**17**) group were found to be the most potent, with their affinity towards D_2 receptor being 26 nM and 27 nM respectively. Interestingly, exchanging 3-methoxy (**17**) with 4-methoxy (**13**) decreased activity three-fold. Within compounds containing indole C5 methoxy group, compound **10** showed two-fold increased affinity compared to **2**, **6**, **14** and **18**. Compounds with furanylmethyl substituent displayed decreased affinity, prominently highlighted by compounds **3** and **4**. This observation suggests the benzyl group contributes favorably towards increased affinity while installation of furanylmethyl is detrimental do the D_2 binding.

In case of 5-HT_{1A} receptors, compounds with methoxy substituent displayed increased affinity with K_i values of 195 nM, 157 nM, 139 nM, 134 nM and 135 nM for compounds **2**, **6**, **10**, **14** and **18** respectively. This contrasts with D_2 affinity where no indole C5 substitution was beneficial for the potency. Increased bulkiness of R_2 group mirrors the trend observed in the case of D_2 affinity, albeit to a lower extent. However, presence of benzyl group at R_1 was beneficial to the 5-HT_{1A} binding, similarly to situation observed in the case of D_2 binding. Furanylmethyl substituent proved again to be the least favorable with the most pronounced effect observed in compound **1** which showed the lowest 5-HT_{1A} affinity (K_i = 752 nM) among all compounds tested. This further corroborates polarizing effect of benzyl and furanylmethyl groups in respect to their effect on affinity.

All compounds were found to have significantly decreased affinity towards 5-HT_{2A} receptor with only **1**, **5**, **9** and **17** displaying potencies in the nanomolar range. These are the compounds without indole C5 substituent, suggesting preference of unsubstituted indole moiety

for the increased affinity in this receptor type. All variations of R_1 tested by us seemed to have limited effect to enhance 5-HT_{2A} binding.

2.5. Receptor functional studies

2.5.1. Functional study of selected multi-target compounds at dopamine D_2 receptors

The functional behavior of compounds **5**, **9** and **17** at dopamine D_2 receptors was investigated in cAMP assays of D_2-mediated inhibition of cAMP production stimulated by forskolin, in CHO-K1 cells expressing the cloned human D_2 receptor. None of the compounds (0.1 nM – 100 μM) was able to inhibit forskolin-stimulated cAMP production, indicative of a lack of D_2 agonist efficacy, while dopamine (1 nM – 1 mM) inhibited forskolin-stimulated cAMP production with an EC_{50} of 40 nM in the same conditions (data not shown). On the contrary, compounds **5**, **9** and **17** (0.1 nM – 100 μM), as well as haloperidol (0.1 nM – 10 μM) included as reference antagonist in the assays, fully antagonized the inhibition of cAMP production elicited by a submaximal (1 μM) concentration of dopamine in a concentration-dependent manner (Supplementary Fig. S6). The potency of the three selected compounds as D_2 antagonists was determined in cAMP assays by Schild analysis of concentration-response curves of the D_2-like receptor full agonist quinpirole (10 pM – 1 mM) in the absence or presence of three different concentrations of the compounds. Compounds **5**, **9** and **17** elicited a parallel rightward shift of the concentration-response curves of quinpirole in a concentration-dependent manner (Fig. 4). Schild plots supported a behavior of competitive antagonism for the three compounds, with fits to linear regression of slope close to unity, and the compounds displayed the same order of potency (pK_b, K_b) (Table 3) than of affinity (K_i) at D_2 receptors.

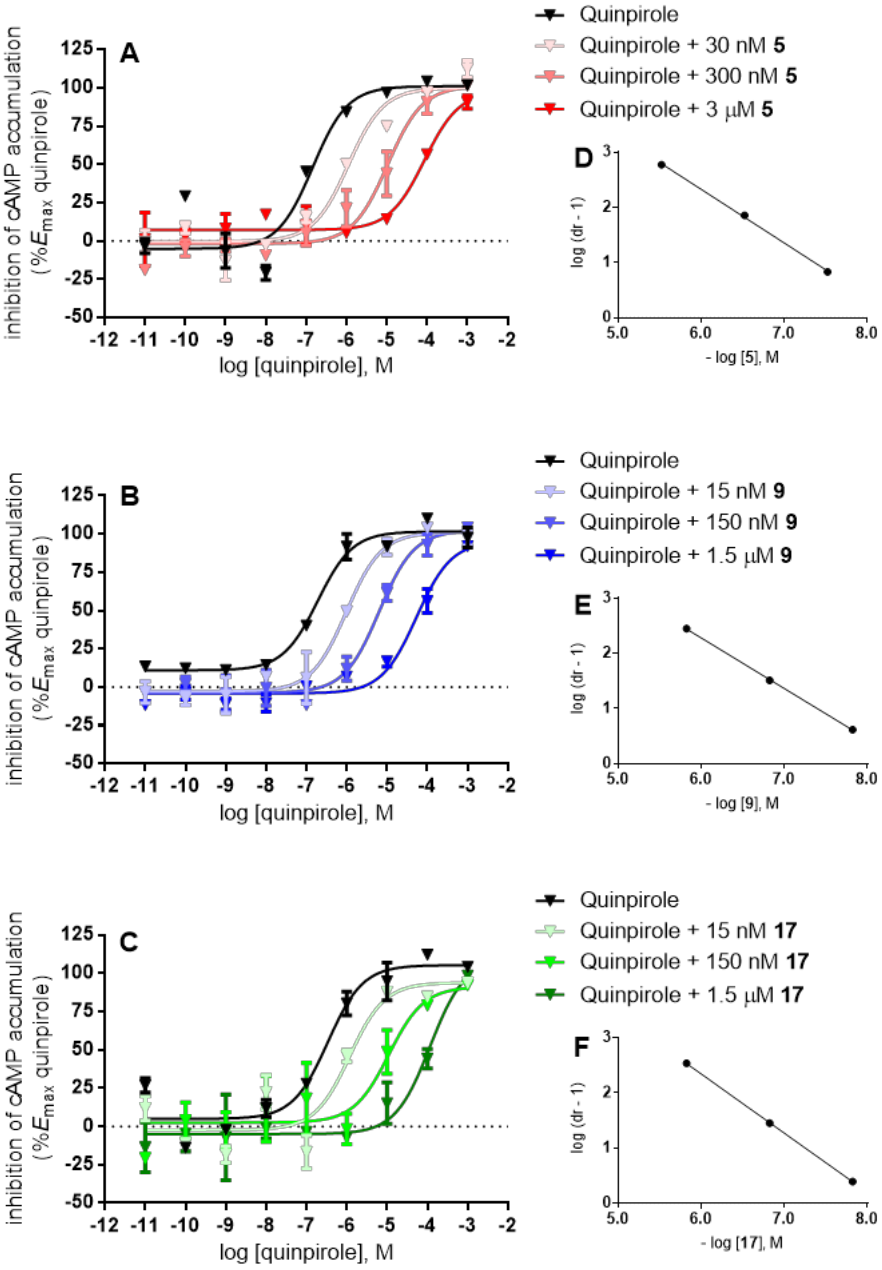

Fig. 4. Functional assays of cAMP signalling at cloned D_2 receptors. Concentration-response (inhibition of forskolin-stimulated cAMP production) curves of quinpirole in the absence or presence of compound **5** (A), **9** (B) or **17** (C) at the indicated concentrations in CHO-K1 cells expressing human D_2 receptors. The graphs show data (mean ± SEM) of one representative experiment out of two independent experiments performed in duplicate. (D, E, F) Schild plots from the experiments shown in A, B and C were fitted to linear regression (R^2 = 0.999, 0.999, and 1.000; slope = 0.972, 1.069, and 1.072, for compounds **5**, **9**, and **17**, respectively).

Table 3. Evaluation of potency and efficacy of selected compounds at the indicated targets in *in vitro* functional assays.[a]

Compound	*h*D_2[a]		*h*5-HT_{1A}[b]	*h*5-HT_{2A}[c]		
	pK_b (mean ± SEM)	K_b [nM]	%E_{max} (mean ± SEM)	max. %inh. (mean ± SEM)	pIC_{50} (mean ± SEM)	IC_{50} [nM]
5	8.30 ± 0.10	5.06	67 ± 9%	96 ± 1%	5.62 ± 0.20	2415
9	8.45 ± 0.03	3.51	89 ± 6%	95 ± 3%	5.58 ± 0.27	2618
17	8.31 ± 0.12	4.95	76 ± 8%	98 ± 2%	5.10 ± 0.22	7980
5-Carboxamidotryptamine	ND[d]	ND	95 ± 3%	ND	ND	ND
Risperidone	ND	ND	ND	99 ± 3%	9.15 ± 0.04	0.72

[a]Antagonism of quinpirole-mediated inhibition of forskolin-stimulated cAMP production in CHO-K1 cells expressing human D_2 receptors. Antagonist potency (pK_b, -logK_b; K_b) was determined by Schild analysis of concentration-response curves of quinpirole in the absence or presence of three different concentrations of the compounds; [b]agonist efficacy (%E_{max}, maximal % of inhibition of forskolin-stimulated cAMP production) in HEK293 cells expressing human 5-HT_{1A} receptors; [c]antagonist efficacy (max. %inh., maximal % of inhibition of 5-HT-stimulated IP production) and potency (pIC_{50}, -log IC_{50}; IC_{50}, concentration of the compound eliciting the 50% of maximal compound effect) in CHO-K1 cells expressing human 5-HT_{2A} receptors; [d]not determined. Data are mean ± SEM of 2 (D_2, 5-HT_{2A}) or 3 (5-HT_{1A}) independent experiments performed in duplicate.

2.5.2. Functional study of selected multi-target compounds at serotonin 5-HT_{1A} and 5-HT_{2A} receptors

The three selected compounds (**5**, **9** and **17**) were evaluated in functional studies at 5-HT_{1A} receptors in cAMP functional assays of 5-HT_{1A}-mediated inhibition of forskolin-stimulated cAMP production, in HEK293 cells stably expressing the cloned human 5-HT_{1A} receptor. The

compounds, assayed at two concentrations (10 µM and 100 µM) inhibited the cAMP production stimulated by forskolin to different extent, indicative of 5-HT_{1A} agonist efficacy. None of the compounds at the concentrations assayed reached the maximal response of the full 5-HT_{1A} agonist 5-CT (Table 3), while concentrations of the compounds higher than 100 µM were not evaluated in order to avoid potential artefacts or solubility issues.

In functional assays of 5-HT_{2A} signalling, any of the three selected compounds showed agonist efficacy at promoting inositol phosphates (IP) production at the concentrations assayed (from 0.1 nM to 10 µM), while 5-HT promoted IP production with EC_{50} of 99 nM in the same assays (data not shown). However, compounds **5**, **9** and **17** completely antagonized 5-HT-stimulated IP production in a concentration-dependent manner (Fig. 5) with IC_{50} values shown in Table 3, resulting compounds **5** and **9** equipotent and compound **17** slightly less potent as 5-HT_{2A} antagonists. K_b values of the three selected compounds as 5-HT_{2A} antagonists estimated following the equation reported by Leff and Dougall [22] (see experimental section) were in the high nanomolar range (K_b (mean ± SEM) = 238 ± 103 nM, 279 ± 154 nM and 803 ± 379 nM for compounds **5**, **9** and **17**, respectively), and they indicated potencies as 5-HT_{2A} antagonists of around 50 times, 80 times and 200 times lower than as D_2 antagonists for compounds **5**, **9** and **17**, respectively.

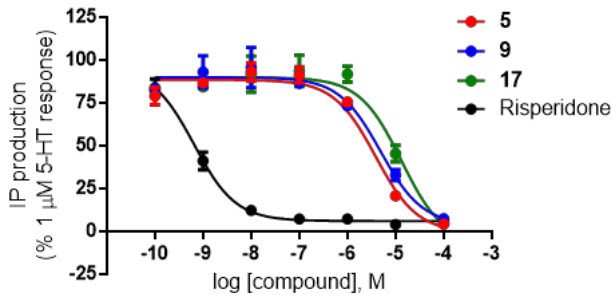

Fig. 5. Functional assays of inositol phosphate signalling at cloned 5-HT_{2A} receptors. Concentration-response curves of compounds **5**, **9**, **17** and risperidone (as reference 5-HT_{2A} antagonist) on IP production stimulated by 1 µM 5-HT in CHO-K1 cells expressing human 5-HT_{2A} receptors. The graph shows data (mean ± SEM) of one representative experiment out of 2 independent experiments performed in duplicate.

2.6. Molecular modeling

In order to study the ligand-receptor interactions at the molecular level, compounds **1-20** were docked to the X-ray structure of the human dopamine D_2 receptor in the inactive state (PDB ID: 6CM4) [23] and previously reported homology models of the human serotonin 5-HT_{1A} and 5-HT_{2A} receptors, also in inactive conformations [9]. In case of all the studied receptors the main ligand-receptor contact was the interaction between the protonatable nitrogen atom of the ligand and the conserved Asp (3.32) (numbering according to Ballesteros-Weinstein nomenclature) [24] of the receptor as typical for orthosteric ligands of aminergic GPCRs [8,9].

The results of molecular docking of most potent compounds **5**, **9** and **17** to the human dopamine D_2 receptor are presented in Fig. 6. The position of ligands in the orthosteric pocket of the D_2 receptor is in accordance with previously reported docking pose for the virtual hit D2AAK1 [8,9] and docking pose of compound **11** (D2AAK1_3) [13]. Indole moiety is directed towards extracellular part of the receptor while the arylmethyl group is placed deeper in the receptor cavity. In addition to interaction with the conserved Asp (3.32) compounds **5**, **9** and **17** interact via π-π stacking interactions with aromatic residues: Trp (6.48), Phe (6.50), Phe (6.51) or Trp 100 from the first extracellular loop, ecl1 or Phe (6.50), Phe (6.51), respectively.

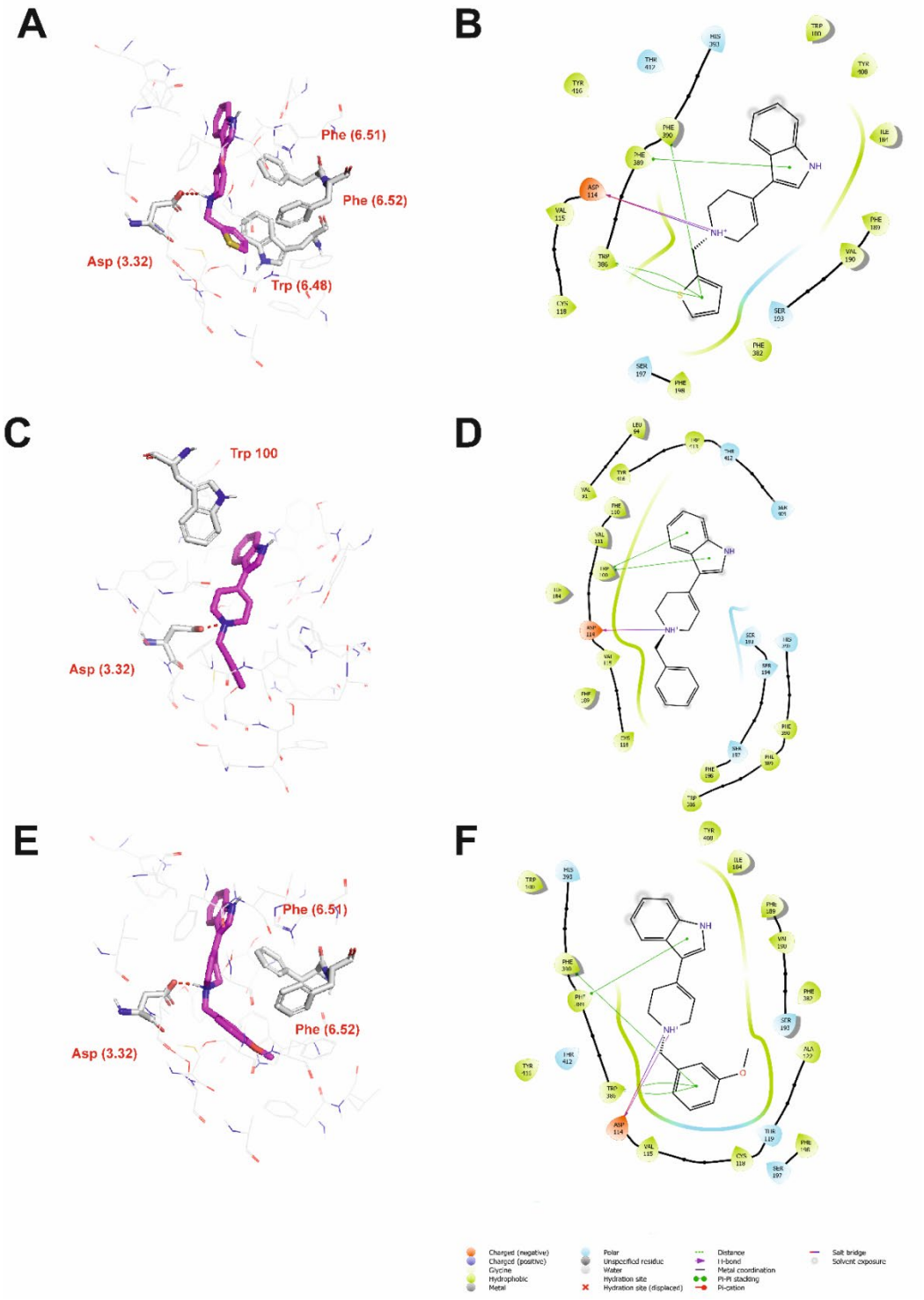

Fig. 6. Compounds **5** (A, B), **9** (C, D) and **17** (E, F) in the binding pocket of human dopamine D_2 receptor. A, C, E – 3D view of the binding site. Ligands represented as sticks with magenta carbon atoms. Protein represented as wire with grey carbon atoms, main interacting residues shown as sticks. Hydrogen bonds shown as red dashed lines. Non-polar hydrogen atoms not shown for clarity. B, D F– 2D view of the binding site.

The results of molecular docking of most potent compounds **5**, **9** and **17** to the human serotonin 5-HT_{1A} receptor are presented in Fig. 7. The ligand poses in this receptor are similar

to the poses at the D_2 receptor and are in agreement with the previously reported pose of the virtual hit D2AAK1 [9]. Compound **9** interacts only with the conserved Asp (3.32) while compounds **5** and **9** form hydrogen bond with Cys 187 from the second extracellular loop, ecl2 and interacts via π-π stacking interaction with Tyr (2.63) and compound **17** forms additional hydrogen bond with Lys 191 from the ecl2 and π-π stacking interaction with Phe (3.28).

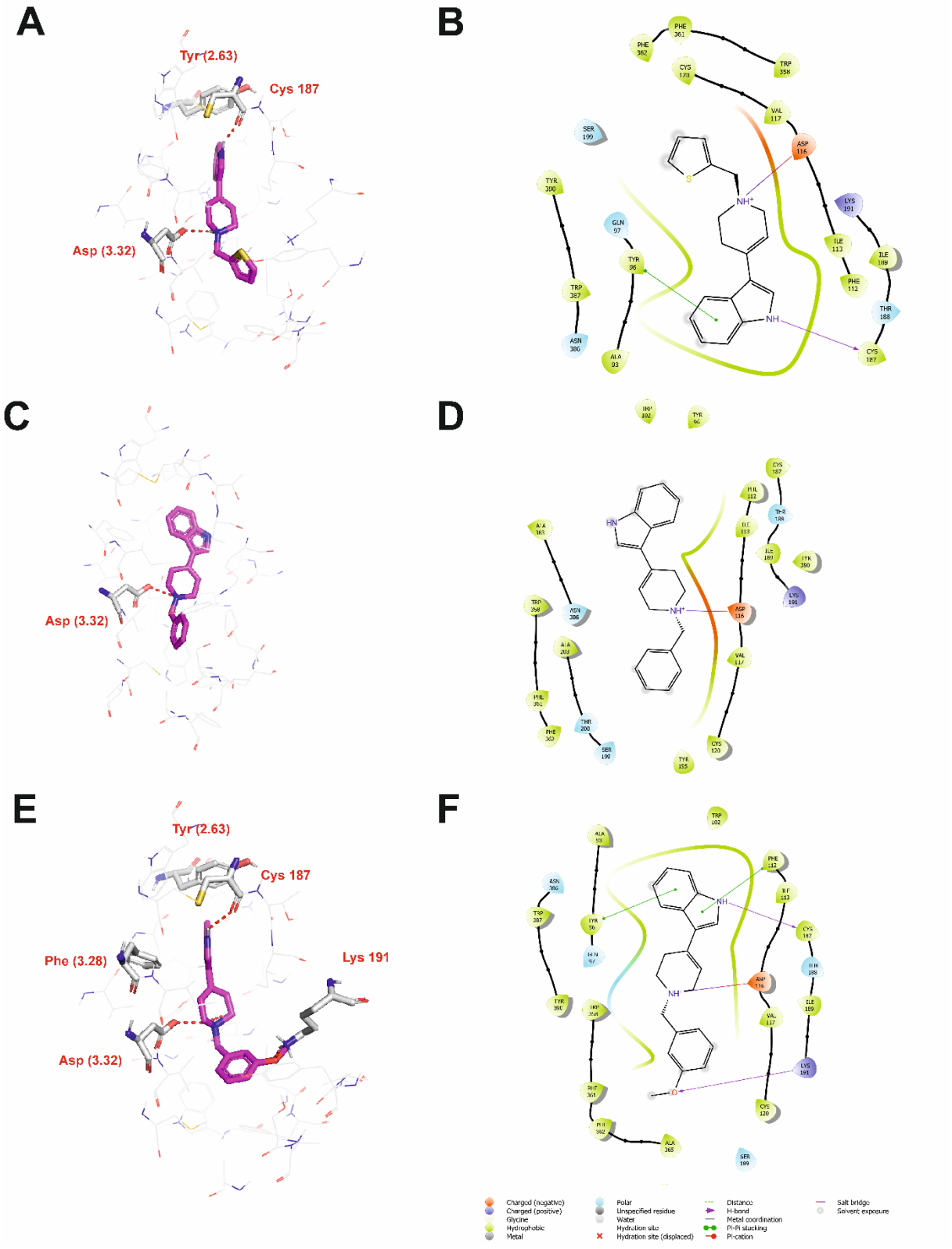

Fig. 7. Compounds **5** (A, B), **9** (C, D) and **17** (E, F) in the binding pocket of human serotonin 5-HT_{1A} receptor. A, C, E – 3D view of the binding site. Ligands represented as sticks with magenta carbon atoms. Protein represented as wire with grey carbon atoms, main interacting residues shown as sticks. Hydrogen bonds shown as red dashed lines. Non-polar hydrogen atoms not shown for clarity. B, D F– 2D view of the binding site.

The results of molecular docking of most potent compounds **5**, **9** and **17** to the human serotonin 5-HT_{2A} receptor are presented in Fig. 8. The docking poses of the studied compounds at this receptor follow the docking poses at the D_2 receptor and 5-HT_{1A} receptor and are in accordance with previously reported docking poses for the virtual hit, D2AAK1 [9]. In addition to interactions with the conserved Asp (3.32), compound **5** forms a hydrogen bond with Cys 227 from the ecl2 and π-π stacking interaction with Trp (3.28) and Phe (6.52), compound **9** interacts via π-π stacking with Trp (3.28) and Phe (6.52) while compound **17** forms a hydrogen bond with Cys 227 from the ecl2 and π-π stacking interaction with Trp (3.28).

Molecular docking partially enabled to explain the observed structure activity relationships of the studied compounds **1**-**20** at the studied receptors. The rationale for a bulky substituent at C5 of the indole moiety was to reduce affinity at dopamine D_2 receptor while keeping the affinity at the serotonin 5-HT_{2A} receptor. From the Glide scoring function it seemed that the effect of unfavorable interactions of alkoxy groups with aqueous environment of the extracellular receptor vestibule is observed to the lesser extent at the studied serotonin receptors. It was only partially confirmed by *in vitro* tests as 5-HT_{2A} receptor affinity was also significantly diminished for compounds with bulky substituents at C5 of the indole moiety. Regarding arylmethyl substituents on the nitrogen atom, the binding pockets of the studied receptors can accommodate all the substituents studied so the simplification of the substituent at this position in comparison to the virtual hit D2AAK1 has minor effect on the ligand affinities at the studied receptors.

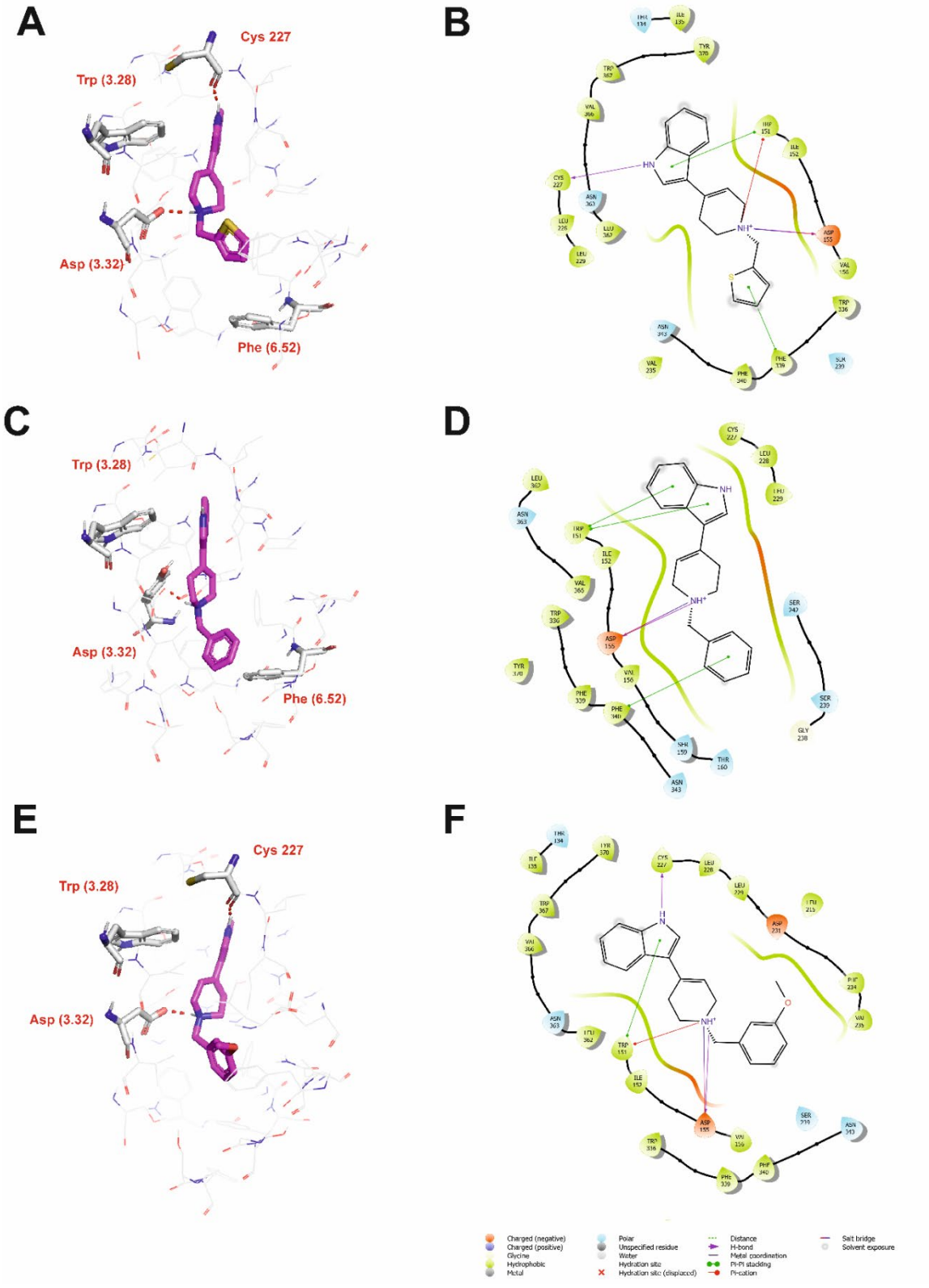

Fig. 8. Compounds **5** (A, B), **9** (C, D) and **17** (E, F) in the binding pocket of human serotonin 5-HT_{2A} receptor. A, C, E – 3D view of the binding site. Ligands represented as sticks with magenta carbon atoms. Protein represented as wire with grey carbon atoms, main interacting residues shown as sticks. Hydrogen bonds shown as red dashed lines. Non-polar hydrogen atoms not shown for clarity. B, D F– 2D view of the binding site.

2.7. Behavioral studies

All compounds studied are characterized by favorable lipophilicity values and are able to cross blood-brain barrier (see Table S1 in Supplementary Information). Compound **5** was selected for the behavioral studies due to most desired multi-receptor profile.

2.7.1. Motor coordination and chimney tests

Compound **5** at the dose investigated (50 mg/kg) did not induce coordination impairments as evaluated in the chimney test (Fig. 9).

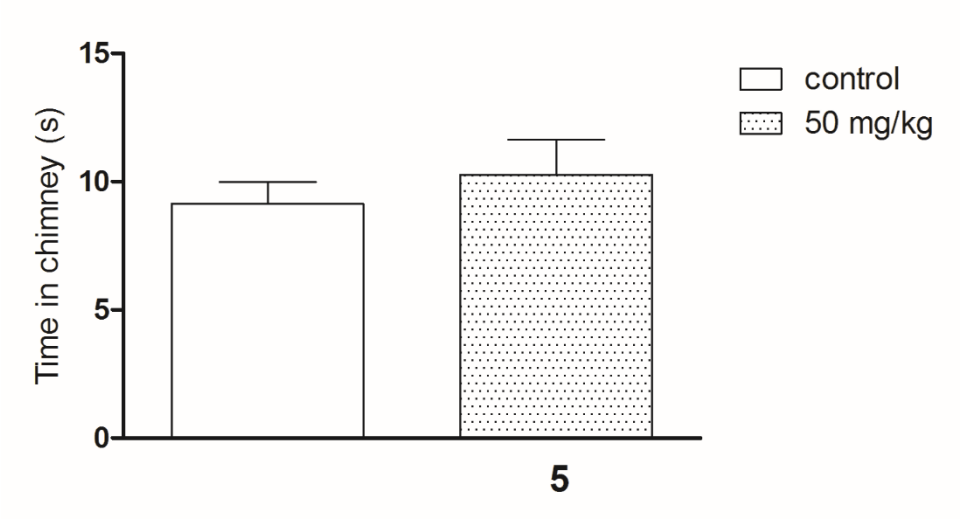

Fig. 9. Influence of the compound **5** on motor coordination in mice evaluated in chimney test. Investigated compound was injected i.p. 60 min before the test. Data are expressed as mean ± SEM values. The *t*-test did not show significant changes in the time in chimney ($p = 0.2253$).

2.7.2. Amphetamine-induced hyperactivity in mice

The effect of **5** on the spontaneous locomotor activity in mice is presented in Fig. 10. Statistical analysis revealed significant changes in the locomotor activity after **5** treatment in combination with amphetamine (two-way ANOVA: pretreatment [$F(1,28)=8.1$, $p<0.01$] and interaction effect between pretreatment and treatment [$F(1,28)=7.59$, $p<0.05$]). The administration of amphetamine increased the locomotor activity of mice vs. saline-treated group ($p<0.01$). Moreover, the post hoc Bonferroni test showed that **5** (50 mg/kg) co-administered

with amphetamine (5 mg/kg) decreased amphetamine-induced hyperactivity when compared to the amphetamine-treated group ($p<0.05$) (Fig. 10).

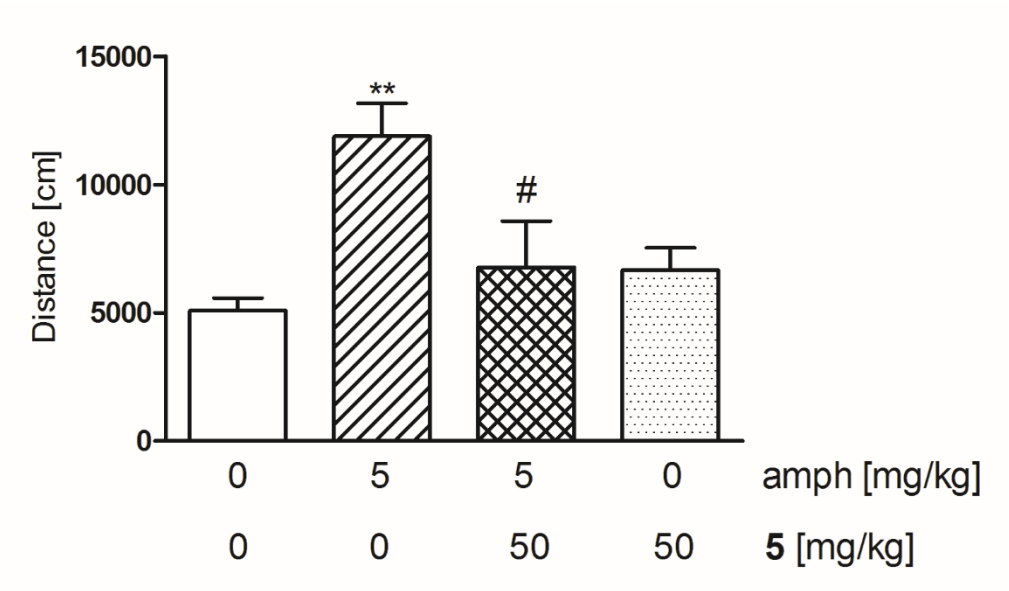

Fig. 10. Influence of **5** on the amphetamine-induced hyperactivity in mice. Appropriate groups of mice received **5** [50 mg/kg, (n = 8); i.p.], amphetamine [5 mg/kg, (n = 8); s.c.], 50 mg/kg of compound **5** and amphetamine (n = 8), and vehicle (n = 8, indicated as 0). Data are presented as mean ± SEM of the distance travelled by mice during 30 min. The results from the Bonferroni test analyses indicate: ** $p < 0.01$ vs. the vehicle-treated group and # $p < 0.05$ vs. amphetamine-treated group.

*2.7.3. Effect of acute administration of **5** (50 mg/kg) on the total duration of immobility in the forced swim test (FST) in mice.*

The influence of **5** (50 mg/kg) on the total duration of immobility was determined in the forced swim test, FST (Fig. 11). The *t-test* revealed the statistically significant decrease in immobility time ($p<0.001$, Fig. 11A) as well as increase in latency time to the first episode of immobility ($p<0.01$) after acute administration of **5** (50 mg/kg; Fig. 11B).

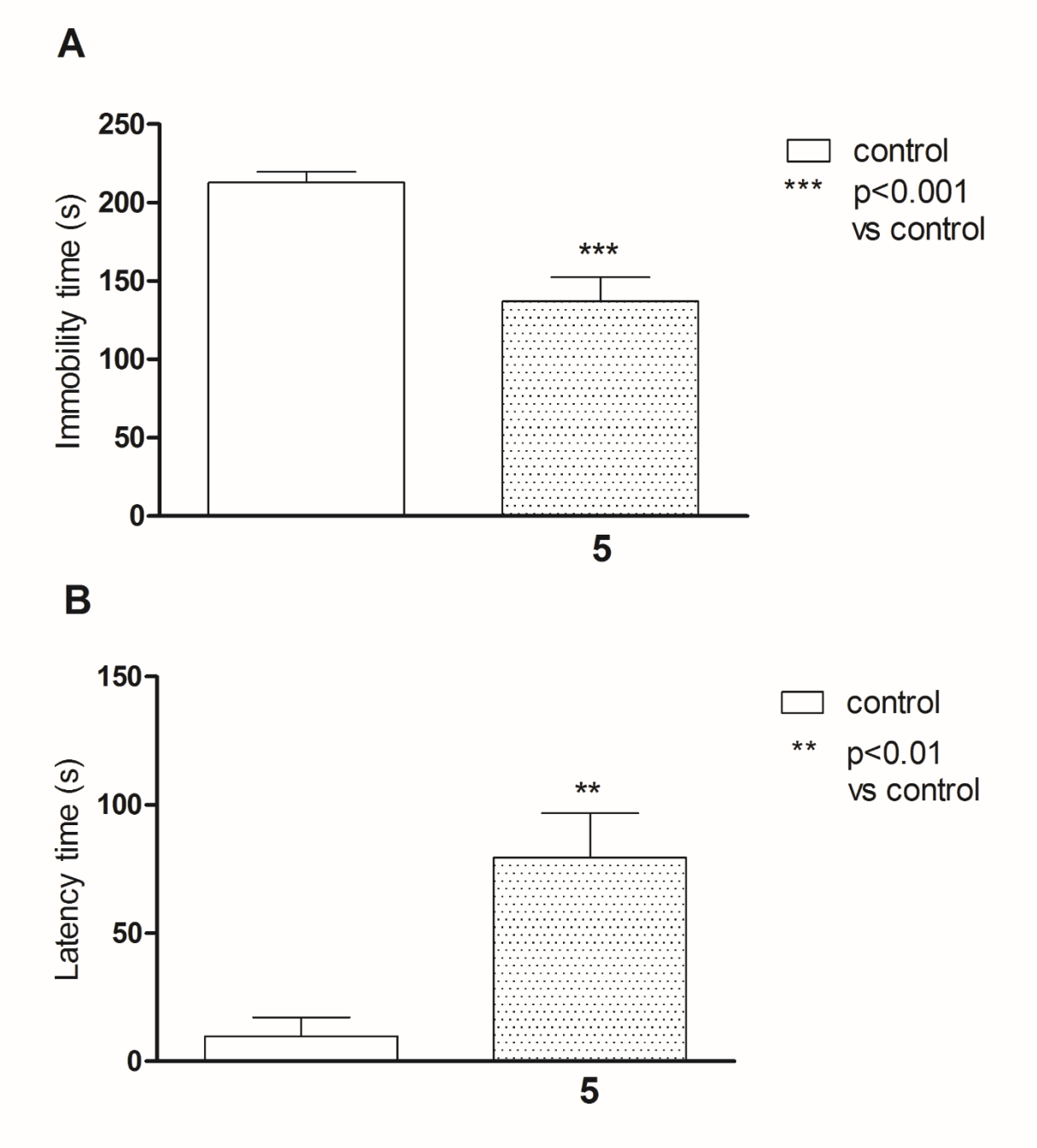

Fig. 11. The influence of the investigated compound **5** (50 mg/kg) on the total duration of immobility in the forced swim test in mice. The investigated compound was administered i.p. 60 min before the test. Data are expressed as mean ± SEM values. The *t*-test showed significant decrease in the immobility time ($p<0.001$) as well as increase in latency time to the first episode of immobility ($p<0.01$) after acute administration of **5** (50 mg/kg).

*2.7.4. Effect of acute administration of **5** on memory consolidation in mice*

The influence of **5** (50 mg/kg) on memory consolidation (Fig. 12) was determined during the retention trial of the passive avoidance (PA) task. *T*-test indicated that the acute administration of studied **5** increased the IL values ($p<0.01$) indicating its pro-cognitive effect.

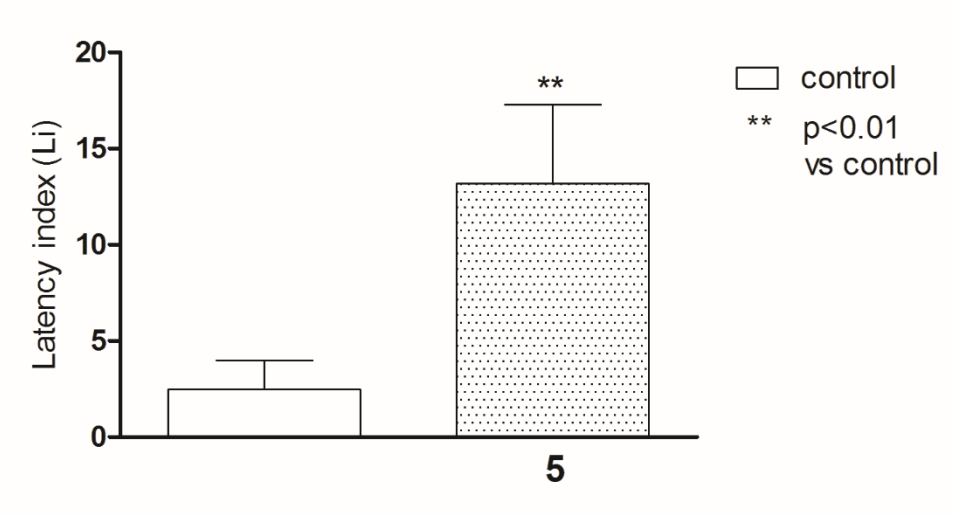

Fig. 12. Compound **5** effects on memory consolidation in mice after an acute administration. Appropriate groups of mice received injections of **5** [50 mg/kg (n = 10) and vehicle (n = 10); i.p.] on Day 1 immediately after the test and the rodents were retested 24 h later (i.e., on Day 2). Data are presented as mean ± SEM. The results from the *t*-test analyses indicate: * $p < 0.01$ vs. the vehicle-treated group.

3. Discussion and conclusions

Schizophrenia is a mental illness of not fully understood pathomechanisms, involving many neurotransmitter systems [4]. This is why selective, one-target drugs are less efficient in the treatment of this disease than second-generation or atypical drugs acting on a number of aminergic GPCRs. Indeed, clozapine which is a gold standard for the treatment-resistant schizophrenia has a nanomolar affinity to several GPCRs [25]. This is a paradigm change from dirty drugs (not beneficial due to possible side effects) to modern multi-target drugs, which are efficient in the treatment of diseases with complex pathomechanism. In accordance to the complex pathomechanism of schizophrenia, the compounds reported here were designed to have affinity for the dopamine D_2 and serotonin 5-HT_{1A} and 5-HT_{2A} receptors, targets of great

importance in schizophrenia. In particular compounds **5**, **9** and **17** display a multi-target profile with nanomolar affinity to all the receptors studied and they can be considered as the post promising compounds in the series.

All antipsychotics currently present at the market are antagonists or partial agonists of the dopamine D_2 receptor. In agreement with this, compounds **5**, **9** and **17** are antagonists of the dopamine D_2 receptor, a mechanism of action well validated as beneficial for the treatment of schizophrenia. Blocking dopamine D_2 receptors enables to treat the positive symptoms of schizophrenia that result from overactivity of D_2 receptors in the mesolimbic dopaminergic pathway (the neuronal projection from the ventral tegmental area (VTA) to the nucleus accumbens, amygdala and hippocampus) [4]. There were attempts to design antipsychotics beyond the dopaminergic hypothesis, however none of these compounds entered the market [1].

Compounds **5**, **9** and **17** are antagonists of the serotonin 5-HT_{2A} receptor, a mechanistic component that has been related with a better clinical performance of atypical antipsychotics at managing negative symptoms of schizophrenia while still being able to control positive symptoms [26]. Indeed, atypical antipsychotics combine high-affinity antagonism of 5-HT_{2A} receptors with D_2 antagonist activity, and in the clinic these drugs resulted superior than typical antipsychotics particularly concerning extrapyramidal side-effects [27], the most serious adverse effects of first generation drugs. The functional data for compounds **5**, **9** and **17** and 5-HT_{1A} receptor are less clear, although they indicate agonism or partial agonism at this receptor, which would be also beneficial for schizophrenia treatment [28]. Detailed discussion of the involvement of dopamine and serotonin receptors in the pathomechanism of schizophrenia is available in our review papers [1,4].

Compounds **1**-**20** were obtained from the reaction of 5-substituted indoles and N-methylarylpperidin-4-ones which is a most convenient method to obtain 3-(1-arylmethyl-

1,2,3,6-tetrahydropyridin-4-yl)-1*H*-indole system [10]. Other approaches to obtain compounds with this skeleton involve the reaction of 1*H*-indolo-2,3-dione with 1-substituted derivatives of piperidin-4-one [29], from the reaction of 3-(piperidin-4-yl)-1*H*-indole with substituted benzyl halides [30] or from the reaction of methyl ester of 2-propenoic acid with substituted benzylamines and indole [31]. Our approach is a simple and convenient one-step procedure and allowed us to obtain high-purity compounds.

One of the most potent compounds, compound **9**, was selected for X-ray studies to get knowledge about its energetically stable conformation in the solid state. The interatomic distances and angles for this compound are in agreement with those described in the literature [12] and are similar to those observed for the other closely related indole derivatives [13–16]. However, the conformation of compound **9** differs from the previously reported conformation of compound **11** (D2AAK1_3), see Fig. 3 [13].

The structure-activity relationship is clear in the reported series of compounds. The bulkiness of 5-alkoxy substituent is not favorable for activity while the effect of N-methyl aryl substituent is less important. The affinities of compounds **1**-**20** to the studied receptors are comparable to previously reported N-alkyl-3-(1-arylmethyl-1,2,3,6-tetrahydropyridin-4-yl)-1*H*-indoles [10,32].

Molecular docking simulations enabled to study ligand-receptor interactions at the molecular level. The docking poses of compounds **1**-**20** in the orthosteric pockets of dopamine D_2 and serotonin 5-HT_{1A} and 5-HT_{2A} receptors are comparable and correspond to the previously reported bonding mode of the virtual hit D2AAK1 [8,9,13] and compound **11** (D2AAK1_3) [13].

Compound **5** with most favorable multi-receptor profile was subjected to *in vivo* investigations. Prior to those the lipophilicity and blood-brain barrier permeation were calculated for all the compounds (see Supplementary Information, Table S1) and all the

compounds were found to cross blood-brain barrier and to have beneficial lipophilicity values. Compound **5** decreased amphetamine-induced hyperactivity in mice which confirms its antipsychotic potential. Moreover, compound **5** increased memory consolidation (pro-cognitive activity) in the passive avoidance test and decreased immobility time in the forced swim test predictive of antidepressant activity. These additional pharmacological activities of compound **5** are extremely relevant due to persistent negative and cognitive symptoms of schizophrenia, which are often retained even between acute schizophrenia episodes. Most probably, antidepressant and pro-cognitive activity of compound **5** is connected with its affinity for serotonin receptors.

In summary, the reported series of multi-target compounds contributes to elaboration of a better treatment for schizophrenia. Effort will be now made to obtain compounds with extended atypical multi-receptor profile and with diminished affinity to off-targets.

4. Experimental section

4.1. Chemistry

All reagents used for synthesis were purchased from commercial suppliers and were used without further purification. NMR spectra were recorded on a Bruker AVANCE III 600 MHz spectrometer equipped with a BBO Z-gradient probe. Spectra were recorded at 25 °C using DMSO-*d6* and $CDCl_3$ as a solvent with a non-spinning sample in 5 mm NMR-tubes. Chemical shifts were expressed in parts per million (ppm) using the solvent signal or TMS as an internal standard. High resolution mass spectra (HRMS) were acquired on a Bruker microTOF-Q II mass spectrometer with electrospray ionization (ESI). Data were processed using MestReNova v.14.0.0 and Compass Data Analysis software. Spectra of the reported compounds can be found in Supplementary Information.

*4.1.1. General procedure for the synthesis of compounds **1 - 20***

A 20 mL vial was charged with 1 mmol of indole, 1.1 mmol of *N*-substituted 4-piperidone and 5 mL of 1M KOH in MeOH. The vial was sealed and the reaction was stirred at 75 °C 18 hours. When precipitate appeared after cooling to room temperature it was filtered and washed with water and diethyl ether and dried. Otherwise, the reaction was stripped of solvent and remaining residue partitioned between water and DCM. Aqueous was extracted with DCM and combined organics washed with brine, dried with anhydrous magnesium sulfate and the crude product was purified by flash column chromatography.

*4.1.1.1. 3-(1-(furan-2-ylmethyl)-1,2,3,6-tetrahydropyridin-4-yl)-1H-indole (**1**)*

Compound precipitated from reaction as a yellow solid. Yield: 69%. Mp 182-186ºC;^{1}H NMR (600 MHz, DMSO) δ 11.11 (s, 1H), 7.80 (d, *J* = 8.0 Hz, 1H), 7.61 (dd, *J* = 1.8, 0.8 Hz, 1H), 7.40 – 7.35 (m, 2H), 7.13 – 7.07 (m, 1H), 7.02 (td, *J* = 7.6, 7.1, 1.0 Hz, 1H), 6.43 (dd, *J* = 3.1, 1.9 Hz, 1H), 6.34 (d, *J* = 3.0 Hz, 1H), 6.11 (t, *J* = 3.5 Hz, 1H), 3.62 (s, 2H), 3.12 (d, *J* = 3.1 Hz, 2H), 2.68 (t, *J* = 5.7 Hz, 2H), 2.54 – 2.51 (m, 2H). ^{13}C NMR (151 MHz, DMSO) δ 152.6, 142.8, 137.4, 130.0, 125.1, 123.2, 121.7, 120.5, 119.7, 117.9, 116.3, 112.2, 110.8, 109.0, 54.3, 52.6, 50.0, 29.0. HRMS (ESI) m/z $[M+H]^+$ calculated for $C_{18}H_{19}N_2O^+$: 279.1492, found: 279.1492.

*4.1.1.2. 3-(1-(furan-2-ylmethyl)-1,2,3,6-tetrahydropyridin-4-yl)-5-methoxy-1H-indole (**2**) [33]*

Compound precipitated from reaction as a yellow solid. Yield: 47%. Mp 183-187ºC; ^{1}H NMR (600 MHz, $CDCl_3$) δ 8.12 (s, 1H), 7.45 – 7.42 (m, 1H), 7.34 (d, *J* = 2.2 Hz, 1H), 7.29 – 7.27 (m, 1H), 7.13 (d, *J* = 2.5 Hz, 1H), 6.88 (dd, *J* = 8.8, 2.4 Hz, 1H), 6.37 (dd, *J* = 2.9, 1.9 Hz, 1H), 6.30 (d, *J* = 3.1 Hz, 1H), 6.16 – 6.11 (m, 1H), 3.87 (s, 3H), 3.74 (s, 2H), 3.31 – 3.26 (m, 2H), 2.81 (t, *J* = 5.8 Hz, 2H), 2.65 – 2.59 (m, 2H). ^{13}C NMR (151 MHz, $CDCl_3$) δ 154.4, 151.9, 142.2, 131.9, 129.8, 125.7, 122.0, 118.7, 117.9, 112.2, 111.9, 110.1, 108.7, 102.9, 56.0, 54.6,

52.6, 49.9, 29.2. HRMS (ESI) m/z $[M+H]^+$ calculated for $C_{19}H_{21}N_2O_2^+$: 309.1598, found: 309.1596.

*4.1.1.3. 5-ethoxy-3-(1-(furan-2-ylmethyl)-1,2,3,6-tetrahydropyridin-4-yl)-1H-indole (**3**)*

Compound precipitated from reaction as a yellow solid. Yield: 66%. Mp 151-155ºC; ^{1}H NMR (600 MHz, DMSO) δ 10.95 (s, 1H), 7.61 (dd, *J* = 1.9, 0.8 Hz, 1H), 7.32 (d, *J* = 2.6 Hz, 1H), 7.25 (d, *J* = 8.7 Hz, 1H), 7.22 (d, *J* = 2.3 Hz, 1H), 6.75 (dd, *J* = 8.7, 2.4 Hz, 1H), 6.43 (dd, *J* = 3.1, 1.9 Hz, 1H), 6.33 (d, *J* = 3.1 Hz, 1H), 6.06 – 6.02 (m, 1H), 4.01 (q, *J* = 6.9 Hz, 2H), 3.61 (s, 2H), 3.13 – 3.09 (m, 2H), 2.67 (t, *J* = 5.7 Hz, 2H), 2.50 – 2.48 (m, 2H), 1.33 (t, *J* = 7.0 Hz, 3H). ^{13}C NMR (151 MHz, DMSO) δ 153.2, 152.6, 142.8, 132.5, 130.1, 125.4, 123.8, 117.5, 116.1, 112.7, 112.1, 110.8, 109.0, 103.6, 63.9, 54.3, 52.6, 50.1, 29.0, 15.4. HRMS (ESI) m/z $[M+H]^+$ calculated for $C_{20}H_{23}N_2O_2^+$: 323.1754, found: 323.1753.

*4.1.1.4. 3-(1-(furan-2-ylmethyl)-1,2,3,6-tetrahydropyridin-4-yl)-5-isopropoxy-1H-indole (**4**)*

Compound precipitated from reaction as a yellow solid. Yield: 43%. Mp 163-166ºC; ^{1}H NMR (600 MHz, $CDCl_3$) δ 8.06 (s, 1H), 7.45 – 7.42 (m, 1H), 7.41 – 7.37 (m, 1H), 7.26 (dd, *J* = 8.7, 1.2 Hz, 1H), 7.15 – 7.12 (m, 1H), 6.89 – 6.86 (m, 1H), 6.39 – 6.36 (m, 1H), 6.31 – 6.28 (m, 1H), 6.14 – 6.10 (m, 1H), 4.57 – 4.49 (m, 1H), 3.73 (s, 2H), 3.31 – 3.24 (m, 2H), 2.84 – 2.77 (m, 2H), 2.66 – 2.59 (m, 2H), 1.36 (d, *J* = 6.1 Hz, 6H). ^{13}C NMR (151 MHz, $CDCl_3$) δ 152.3, 152.0, 142.2, 132.2, 129.7, 125.8, 122.0, 118.8, 117.9, 114.4, 111.7, 110.1, 108.7, 107.4, 71.6, 54.6, 52.6, 49.9, 29.1, 22.3. HRMS (ESI) m/z $[M+H]^+$ calculated for $C_{21}H_{25}N_2O_2^+$: 337.1911, found: 337.1912.

*4.1.1.5. 3-(1-(thiophen-2-ylmethyl)-1,2,3,6-tetrahydropyridin-4-yl)-1H-indole (**5**)*

Compound precipitated from reaction as a yellow solid. Yield: 69%. Mp 170-174ºC; ^{1}H NMR (600 MHz, DMSO) δ 11.11 (s, 1H), 7.81 (d, *J* = 8.0 Hz, 1H), 7.45 (dd, *J* = 5.1, 1.3 Hz, 1H), 7.39 – 7.36 (m, 2H), 7.12 – 7.08 (m, 1H), 7.04 – 6.98 (m, 3H), 6.12 (t, *J* = 3.5 Hz, 1H), 3.81 (s, 2H), 3.17 (q, *J* = 2.3 Hz, 2H), 2.69 (t, *J* = 5.7 Hz, 2H), 2.52 (s, 2H). ^{13}C NMR (151 MHz, DMSO) δ 142.7, 137.4, 130.1, 127.0, 126.3, 125.8, 125.1, 123.2, 121.7, 120.5, 119.7, 117.9, 116.3, 112.2, 56.7, 53.0, 50.0, 29.0. HRMS (ESI) m/z $[M+H]^+$ calculated for $C_{18}H_{19}N_2S^+$: 295.1263, found: 295.1264.

*4.1.1.6. 5-methoxy-3-(1-(thiophen-2-ylmethyl)-1,2,3,6-tetrahydropyridin-4-yl)-1H-indole (**6**)*

Compound precipitated from reaction as a brown solid. Yield: 42%. Mp 221-223ºC;^{1}H NMR (600 MHz, DMSO) δ 10.98 (s, 1H), 7.45 (dd, *J* = 5.1, 1.3 Hz, 1H), 7.34 (d, *J* = 2.6 Hz, 1H), 7.27 (d, *J* = 8.7 Hz, 1H), 7.24 (d, *J* = 2.4 Hz, 1H), 7.02 (dd, *J* = 3.4, 1.0 Hz, 1H), 6.99 (dd, *J* = 5.1, 3.4 Hz, 1H), 6.76 (dd, *J* = 8.7, 2.4 Hz, 1H), 6.07 (t, *J* = 3.5 Hz, 1H), 3.80 (s, 2H), 3.76 (s, 3H), 3.16 (d, *J* = 3.1 Hz, 2H), 2.69 (t, *J* = 5.7 Hz, 2H), 2.50 (s, 2H). ^{13}C NMR (151 MHz, DMSO) δ 154.1, 142.7, 132.5, 130.2, 127.0, 126.4, 125.9, 125.3, 123.9, 117.5, 116.1, 112.8, 111.7, 102.6, 56.7, 55.9, 53.0, 50.0, 29.0. HRMS (ESI) m/z $[M+H]^+$ calculated for $C_{19}H_{21}N_2OS^+$: 325.1369, found: 325.1369.

*4.1.1.7. 5-ethoxy-3-(1-(thiophen-2-ylmethyl)-1,2,3,6-tetrahydropyridin-4-yl)-1H-indole (**7**)*

Compound precipitated from reaction as a beige solid. Yield: 66%. Mp 170-174ºC;^{1}H NMR (600 MHz, DMSO) δ 10.95 (s, 1H), 7.44 (dd, *J* = 5.1, 1.3 Hz, 1H), 7.32 (d, *J* = 2.6 Hz, 1H), 7.25 (d, *J* = 8.7 Hz, 1H), 7.23 (d, *J* = 2.3 Hz, 1H), 7.02 – 7.00 (m, 1H), 7.00 – 6.97 (m, 1H), 6.75 (dd, *J* = 8.7, 2.4 Hz, 1H), 6.05 (t, *J* = 3.5 Hz, 1H), 4.01 (q, *J* = 7.0 Hz, 2H), 3.79 (s, 2H), 3.18 – 3.13 (m, 2H), 2.68 (t, *J* = 5.7 Hz, 2H), 2.49 (s, 2H), 1.32 (t, *J* = 7.0 Hz, 3H). ^{13}C NMR

(151 MHz, DMSO) δ 152.7, 142.2, 132.0, 129.6, 126.4, 125.8, 125.3, 124.8, 123.3, 116.9, 115.5, 112.1, 111.5, 103.1, 63.3, 56.1, 52.4, 49.4, 28.4, 14.8. HRMS (ESI) m/z $[M+H]^+$ calculated for $C_{20}H_{23}N_2OS^+$: 339.1526, found: 325.1525.

*4.1.1.8. 5-isopropoxy-3-(1-(thiophen-2-ylmethyl)-1,2,3,6-tetrahydropyridin-4-yl)-1H-indole (**8**)*

Compound precipitated from reaction as a beige solid. Yield: 44%. Mp 140-143ºC; ^{1}H NMR (600 MHz, DMSO) δ 10.94 (s, 1H), 7.44 (dd, *J* = 5.1, 1.3 Hz, 1H), 7.32 (d, *J* = 2.6 Hz, 1H), 7.26 – 7.24 (m, 2H), 7.02 – 7.00 (m, 1H), 7.00 – 6.97 (m, 1H), 6.75 (dd, *J* = 8.8, 2.3 Hz, 1H), 6.03 (t, *J* = 3.5 Hz, 1H), 4.53 (hept, *J* = 6.1 Hz, 1H), 3.79 (s, 2H), 3.17 – 3.14 (m, 2H), 2.67 (t, *J* = 5.7 Hz, 2H), 2.50 – 2.48 (m, 2H), 1.24 (d, *J* = 6.0 Hz, 6H). ^{13}C NMR (151 MHz, DMSO) δ 151.3, 142.2, 132.2, 129.6, 126.4, 125.8, 125.3, 124.9, 123.4, 116.9, 115.4, 113.0, 112.1, 106.2, 70.2, 56.1, 52.4, 49.4, 28.4, 22.0. HRMS (ESI) m/z $[M+H]^+$ calculated for $C_{21}H_{25}N_2OS^+$: 353.1682, found: 353.1697.

*4.1.1.9. 3-(1-benzyl-1,2,3,6-tetrahydropyridin-4-yl)-1H-indole (**9**) [34]*

*Compound precipitated from reaction as a yellow solid. Yield: 26%. Mp 164-169ºC;^{1}H NMR (600 MHz, DMSO) δ 11.10 (s, 1H), 7.80 (d, J = 8.0 Hz, 1H), 7.39 – 7.33 (m, 6H), 7.29 – 7.25 (m, 1H), 7.10 (ddd, J = 8.1, 7.1, 1.0 Hz, 1H), 7.02 (ddd, J = 8.1, 7.0, 1.1 Hz, 1H), 6.12 (t, J = 3.5 Hz, 1H), 3.60 (s, 2H), 3.11 (q, J = 2.4 Hz, 2H), 2.66 (t, J = 5.7 Hz, 2H), 2.53 – 2.51 (m, 2H). ^{13}C NMR (151 MHz, DMSO) δ 139.1, 137.4, 130.1, 129.3, 128.7, 127.4, 125.1, 123.2, 121.7, 120.6, 119.7, 118.1, 116.4, 112.2, 62.5, 53.3, 50.3, 29.1. HRMS (ESI) m/z $[M+H]^+$ calculated for $C_{20}H_{21}N_2^+$: 289.1699, found: 289.17124.1.1.10. 3-(1-benzyl-1,2,3,6-tetrahydropyridin-4-yl)-5-methoxy-1H-indole (**10**) [34]*

Compound precipitated from reaction as a yellow solid. Yield: 73%. Mp 174-176ºC; ^{1}H NMR (600 MHz, DMSO) δ 10.96 (s, 1H), 7.39 – 7.32 (m, 5H), 7.30 – 7.25 (m, 2H), 7.23 (d, *J* = 2.2 Hz, 1H), 6.75 (dd, *J* = 8.7, 2.3 Hz, 1H), 6.09 – 6.05 (m, 1H), 3.76 (s, 3H), 3.59 (s, 2H), 3.12 –

3.09 (m, 2H), 2.66 (t, *J* = 5.7 Hz, 2H), 2.51 (s, 2H). ^{13}C NMR (151 MHz, DMSO) δ 154.1, 139.1, 132.5, 130.2, 129.3, 128.7, 127.4, 125.4, 123.8, 117.7, 116.1, 112.8, 111.7, 102.6, 62.6, 55.9, 53.3, 50.4, 29.1. HRMS (ESI) m/z $[M+H]^+$ calculated for $C_{21}H_{23}N_2O^+$: 319.1805, found: 319.1819.

*4.1.1.11. 3-(1-benzyl-1,2,3,6-tetrahydropyridin-4-yl)-5-ethoxy-1H-indole (**11**) [13]*

Compound precipitated from reaction as a yellow solid. Yield: 46%. Mp 187-191ºC;^{1}H NMR (600 MHz, DMSO) δ 10.94 (s, 1H), 7.38 – 7.33 (m, 4H), 7.32 (d, *J* = 2.6 Hz, 1H), 7.29 – 7.24 (m, 2H), 7.22 (d, *J* = 2.3 Hz, 1H), 6.75 (dd, *J* = 8.7, 2.3 Hz, 1H), 6.05 (t, *J* = 3.3 Hz, 1H), 4.01 (q, *J* = 6.9 Hz, 2H), 3.59 (s, 2H), 3.12 – 3.08 (m, 2H), 2.65 (t, *J* = 5.7 Hz, 2H), 2.50 (s, 2H), 1.32 (t, *J* = 7.0 Hz, 3H). ^{13}C NMR (151 MHz, DMSO) δ 153.2, 139.1, 132.5, 130.1, 129.3, 128.7, 127.4, 125.4, 123.8, 117.7, 116.1, 112.7, 112.1, 103.7, 63.9, 62.6, 53.3, 50.4, 29.1, 15.4. HRMS (ESI) m/z $[M+H]^+$ calculated for $C_{22}H_{25}N_2O^+$: 333.1961, found: 319.1964.

*4.1.1.12. 3-(1-benzyl-1,2,3,6-tetrahydropyridin-4-yl)-5-isopropoxy-1H-indole (**12**)*

Compound precipitated from reaction as a yellow solid. Yield: 36%. Mp 147-149ºC; ^{1}H NMR (600 MHz, DMSO) δ 10.95 (s, 1H), 7.39 – 7.31 (m, 5H), 7.29 – 7.23 (m, 3H), 6.75 (dd, *J* = 8.8, 2.2 Hz, 1H), 6.04 (t, *J* = 3.4 Hz, 1H), 4.53 (hept, *J* = 6.0 Hz, 1H), 3.58 (s, 2H), 3.12 – 3.08 (m, 2H), 2.65 (t, *J* = 5.7 Hz, 2H), 2.51 – 2.48 (m, 2H), 1.24 (d, *J* = 6.0 Hz, 6H). ^{13}C NMR (151 MHz, DMSO) δ 151.8, 139.1, 132.8, 130.1, 129.3, 128.6, 127.4, 125.5, 123.9, 117.6, 116.0, 113.6, 112.7, 106.7, 70.7, 62.6, 53.3, 50.3, 29.1, 22.5. HRMS (ESI) m/z $[M+H]^+$ calculated for $C_{23}H_{27}N_2O^+$: 347.2118, found: 347.2117.

*4.1.1.13. 3-(1-(4-methoxybenzyl)-1,2,3,6-tetrahydropyridin-4-yl)-1H-indole (**13**) [31]*

Compound precipitated from reaction as a yellow solid. Yield: 10%. Mp 186-190ºC; ^{1}H NMR (600 MHz, DMSO) δ 11.11 (s, 1H), 7.79 (d, *J* = 8.0 Hz, 1H), 7.40 – 7.35 (m, 2H), 7.27 (d, *J* =

8.6 Hz, 2H), 7.12 – 7.08 (m, 1H), 7.02 (ddd, *J* = 8.0, 7.1, 1.0 Hz, 1H), 6.90 (d, *J* = 8.7 Hz, 2H), 6.11 (t, *J* = 3.5 Hz, 1H), 3.75 (s, 3H), 3.52 (s, 2H), 3.10 – 3.06 (m, 2H), 2.63 (t, *J* = 5.7 Hz, 2H), 2.50 – 2.49 (m, 2H). ^{13}C NMR (151 MHz, DMSO) δ 158.7, 137.4, 130.9, 130.5, 130.1, 125.1, 123.2, 121.7, 120.5, 119.7, 118.1, 116.4, 114.0, 112.2, 61.9, 55.5, 53.2, 50.1, 29.1. HRMS (ESI) m/z $[M+H]^+$ calculated for $C_{21}H_{23}N_2O^+$: 319.1805, found: 319.1812.

*4.1.1.14. 5-methoxy-3-(1-(4-methoxybenzyl)-1,2,3,6-tetrahydropyridin-4-yl)-1H-indole (**14**) [31]*

Compound precipitated from reaction as a yellow solid. Yield: 39%. Mp 148-151ºC; ^{1}H NMR (600 MHz, DMSO) δ 10.95 (s, 1H), 7.32 (d, *J* = 2.6 Hz, 1H), 7.28 – 7.25 (m, 3H), 7.22 (d, *J* = 2.4 Hz, 1H), 6.93 – 6.88 (m, 2H), 6.75 (dd, *J* = 8.7, 2.4 Hz, 1H), 6.06 (t, *J* = 3.6 Hz, 1H), 3.76 (s, 3H), 3.75 (s, 3H), 3.52 (s, 2H), 3.10 – 3.05 (m, 2H), 2.63 (t, *J* = 5.7 Hz, 2H), 2.51 – 2.47 (m, 2H). ^{13}C NMR (151 MHz, DMSO) δ 158.7, 154.1, 132.5, 130.9, 130.5, 130.2, 125.4, 123.8, 117.7, 116.2, 114.0, 112.8, 111.7, 102.6, 62.0, 55.9, 55.5, 53.2, 50.2, 29.1. HRMS (ESI) m/z $[M+H]^+$ calculated for $C_{22}H_{25}N_2O_2^+$: 349.1911, found: 349.1917.

*4.1.1.15. 5-ethoxy-3-(1-(4-methoxybenzyl)-1,2,3,6-tetrahydropyridin-4-yl)-1H-indole (**15**)*

Compound precipitated from reaction as a beige solid. Yield: 30%. Mp 133-136ºC; ^{1}H NMR (600 MHz, DMSO) δ 10.95 (s, 1H), 7.31 (d, *J* = 2.6 Hz, 1H), 7.29 – 7.24 (m, 3H), 7.22 (d, *J* = 2.3 Hz, 1H), 6.93 – 6.88 (m, 2H), 6.74 (dd, *J* = 8.7, 2.4 Hz, 1H), 6.04 (t, *J* = 3.5 Hz, 1H), 4.01 (q, *J* = 7.0 Hz, 2H), 3.75 (s, 3H), 3.51 (s, 2H), 3.09 – 3.05 (m, 2H), 2.62 (t, *J* = 5.7 Hz, 2H), 2.50 – 2.46 (m, 2H), 1.32 (t, *J* = 7.0 Hz, 3H). ^{13}C NMR (151 MHz, DMSO) δ 158.1, 152.7, 132.0, 130.3, 129.9, 129.6, 124.8, 123.2, 117.1, 115.5, 113.4, 112.1, 111.5, 103.1, 63.3, 61.4, 54.9, 52.6, 49.6, 28.5, 14.8. HRMS (ESI) m/z $[M+H]^+$ calculated for $C_{23}H_{27}N_2O_2^+$: 363.2067, found: 363.2062.

*4.1.1.16. 5-isopropoxy-3-(1-(4-methoxybenzyl)-1,2,3,6-tetrahydropyridin-4-yl)-1H-indole (**16**)*

Compound precipitated from reaction as an orange solid. Yield: 20%. Mp 146-149ºC; ^{1}H NMR (600 MHz, DMSO) δ 10.95 (s, 1H), 7.31 (s, 1H), 7.28 – 7.22 (m, 4H), 6.92 – 6.88 (m, 2H), 6.74 (dd, *J* = 8.7, 2.3 Hz, 1H), 6.02 (t, *J* = 3.4 Hz, 1H), 4.52 (hept, *J* = 6.1 Hz, 1H), 3.74 (s, 3H), 3.51 (s, 2H), 3.09 – 3.04 (m, 2H), 2.62 (t, *J* = 5.7 Hz, 2H), 2.49 – 2.45 (m, 2H), 1.23 (d, *J* = 6.0 Hz, 6H). ^{13}C NMR (151 MHz, DMSO) δ 158.7, 151.8, 132.8, 130.9, 130.5, 130.1, 125.5, 123.9, 117.7, 116.0, 114.0, 113.6, 112.7, 106.7, 70.7, 61.9, 55.5, 53.2, 50.2, 29.1, 22.5. HRMS (ESI) m/z $[M+H]^+$ calculated for $C_{24}H_{29}N_2O_2^+$: 377.2224, found: 377.2223.

*4.1.1.17. 3-(1-(3-methoxybenzyl)-1,2,3,6-tetrahydropyridin-4-yl)-1H-indole (**17**)*

Compound precipitated from reaction as a beige solid. Yield: 27%. Mp 140-144ºC; ^{1}H NMR (600 MHz, DMSO) δ 11.10 (s, 1H), 7.80 (d, *J* = 8.0 Hz, 1H), 7.40 – 7.35 (m, 2H), 7.26 (t, *J* = 7.8 Hz, 1H), 7.13 – 7.08 (m, 1H), 7.02 (ddd, *J* = 8.0, 7.1, 1.0 Hz, 1H), 6.97 – 6.91 (m, 2H), 6.86 – 6.81 (m, 1H), 6.13 (t, *J* = 3.3 Hz, 1H), 3.76 (s, 3H), 3.57 (s, 2H), 3.14 – 3.09 (m, 2H), 2.65 (t, *J* = 5.7 Hz, 2H), 2.54 – 2.52 (m, 2H). ^{13}C NMR (151 MHz, DMSO) δ 159.8, 140.8, 137.4, 130.1, 129.7, 125.1, 123.2, 121.7, 121.4, 120.6, 119.7, 118.1, 116.4, 114.5, 112.9, 112.2, 62.4, 55.4, 53.3, 50.3, 29.0. HRMS (ESI) m/z $[M+H]^+$ calculated for $C_{21}H_{23}N_2O^+$: 319.1805, found: 319.1805.

*4.1.1.18. 5-methoxy-3-(1-(3-methoxybenzyl)-1,2,3,6-tetrahydropyridin-4-yl)-1H-indole (**18**)*

Compound precipitated from reaction as a yellow solid. Yield: 33%. Mp: 167-171ºC; ^{1}H NMR (600 MHz, DMSO) δ 10.96 (s, 1H), 7.33 (d, *J* = 2.6 Hz, 1H), 7.29 – 7.22 (m, 3H), 6.96 – 6.91 (m, 2H), 6.84 (dd, *J* = 8.0, 2.4 Hz, 1H), 6.76 (dd, *J* = 8.7, 2.4 Hz, 1H), 6.10 – 6.05 (m, 1H), 3.76 (s, 3H), 3.76 (s, 3H), 3.57 (s, 2H), 3.13 – 3.09 (m, 2H), 2.65 (t, *J* = 5.7 Hz, 2H), 2.51 (s, 2H). ^{13}C NMR (151 MHz, DMSO) δ 159.7, 154.1, 140.8, 132.5, 130.2, 129.7, 125.3, 123.9, 121.5,

117.7, 116.1, 114.6, 112.8, 112.8, 111.7, 102.6, 62.5, 55.9, 55.4, 53.3, 50.3, 29.1. HRMS (ESI) m/z $[M+H]^+$ calculated for $C_{22}H_{25}N_2O_2^+$: 349.1911, found: 349.1910.

*4.1.1.19. 5-ethoxy-3-(1-(3-methoxybenzyl)-1,2,3,6-tetrahydropyridin-4-yl)-1H-indole (**19**)*

Compound precipitated from reaction as a yellow solid. Yield: 55%. Mp 133-136ºC; ^{1}H NMR (600 MHz, DMSO) δ 10.94 (s, 1H), 7.32 (d, *J* = 2.6 Hz, 1H), 7.28 – 7.22 (m, 3H), 6.95 – 6.92 (m, 2H), 6.85 – 6.82 (m, 1H), 6.75 (dd, *J* = 8.7, 2.4 Hz, 1H), 6.06 (t, *J* = 3.5 Hz, 1H), 4.01 (q, *J* = 7.0 Hz, 2H), 3.76 (s, 3H), 3.56 (s, 2H), 3.13 – 3.09 (m, 2H), 2.65 (t, *J* = 5.7 Hz, 2H), 2.51 – 2.48 (m, 2H), 1.33 (t, *J* = 7.0 Hz, 3H). ^{13}C NMR (151 MHz, DMSO) δ 159.2, 152.7, 140.2, 132.0, 129.6, 129.1, 124.8, 123.2, 120.9, 117.1, 115.5, 114.0, 112.3, 112.1, 111.5, 103.2, 63.3, 61.9, 54.8, 52.8, 49.8, 28.5, 14.8. HRMS (ESI) m/z $[M+H]^+$ calculated for $C_{23}H_{27}N_2O_2^+$: 363.2067, found: 363.2066.

*4.1.1.20. 5-isopropoxy-3-(1-(3-methoxybenzyl)-1,2,3,6-tetrahydropyridin-4-yl)-1H-indole (**20**)*

Compound was purified by flash column chromatography eluting with 2-5% 2M NH_3/MeOH in DCM and obtained as a yellow oil. Yield: 52%. ^{1}H NMR (600 MHz, DMSO) δ 10.94 (s, 1H), 7.32 (d, *J* = 2.6 Hz, 1H), 7.27 – 7.23 (m, 3H), 6.95 – 6.91 (m, 2H), 6.85 – 6.81 (m, 1H), 6.74 (dd, *J* = 8.8, 2.2 Hz, 1H), 6.03 (t, *J* = 3.4 Hz, 1H), 4.53 (hept, *J* = 6.0 Hz, 1H), 3.75 (s, 3H), 3.56 (s, 2H), 3.12 – 3.08 (m, 2H), 2.64 (t, *J* = 5.7 Hz, 2H), 2.50 – 2.47 (m, 2H), 1.24 (d, *J* = 6.0 Hz, 6H). ^{13}C NMR (151 MHz, DMSO) δ 159.2, 151.2, 140.2, 132.2, 129.6, 129.1, 124.9, 123.3, 120.9, 117.1, 115.4, 114.0, 113.0, 112.3, 112.1, 106.1, 70.2, 61.9, 54.8, 52.7, 49.7, 28.5, 22.0. HRMS (ESI) m/z $[M+H]^+$ calculated for $C_{24}H_{29}N_2O_2^+$: 377.2224, found: 377.2226.

4.2. X-ray studies

The X-ray single crystal measurement at 298 K was performed on an Xcalibur CCD diffractometer with graphite monochromated MoKα (λ = 0.71073 A) radiation. The ω-scan technique was used for data collection. The Oxford Diffraction software CrysAlis CCD and CrysAlis RED programs [35] were used during the data collection, cell refinement and data reduction processes. A multi-scan absorption correction was applied, and the data were corrected for Lorentz and polarization effects. The solution and refinement of the structure was performed with the programs SHELXS-2013 and SHELXL-2013 [36] implemented in the WINGX software package [37]. Non H atoms were refined with anisotropic displacement parameters. All hydrogen atoms bonded to carbon were included in the model at geometrically calculated positions (C–H = 0.93–0.97 Å) and refined using a riding model with U_{iso}(H) = 1.2 or 1.5 U_{eq}(C). The N–H hydrogen atom was located in a difference-Fourier map and refined isotropically. The geometrical calculations were performed using the PLATON program [38]. A summary of crystal data, experimental and refinement details are given in Supplementary Table S2. The bond distances and selected angles are listed in Supplementary Table S3. The molecular structures were drawn with ORTEP3 for Windows [39] and Mercury [40]. Crystallographic data for **9** have been deposited at the Cambridge Crystallographic Data Centre with the deposition number CCDC 1918532. Copies of the data can be obtained free of charge from The Cambridge Crystallographic Data Centre *via* www.ccdc.cam.ac.uk/data request/cif.

Table 4.

4.3. Receptor binding assays

D_2 and 5-HT_{2A} receptor binding assays were performed in membranes from Chinese Hamster Ovary K1 (CHO-K1) cells stably expressing the cloned human D_{2S} (isoform D_{2short}) [25] and 5-HT_{2A} [41] receptors that have been previously described, whereas 5-HT_{1A} receptor binding assays were performed in membranes from Human Embryonic Kidney 293 (HEK293)

cells stably expressing the cloned human receptor previously employed [9,42]. Competition binding experiments at the different receptors were performed with 6 different concentrations of the compounds and following previously described binding procedures [8] with minor modifications (Supplementary Information, Table S4). In brief, 0.2 nM [^{3}H]-Spiperone (D_2), 1 nM [^{3}H]-8-OH-DPAT (5-HT_{1A}) and 1 nM [^{3}H]-Ketanserin (5-HT_{2A}) were employed as radioligands. Non-specific binding was assessed in the presence of 10 µM sulpiride (D_2), 10 µM serotonin (5-HT_{1A}) and 1 µM methysergide (5-HT_{2A}). Affinity (equilibrium dissociation constants (K_i) and logK_i values) were calculated using Prism 6 software (GraphPad, San Diego, CA), by fitting the data from competition binding curves to a single binding site competition model using the equations logEC50 = log(10^logKi*(1+HotNM/HotKdNM)) and Y = Bottom + (Top - Bottom)/(1+10^(XLogEC50)), where Y is binding, HotNM is the concentration of radioligand in the assay, HotKdNM is the equilibrium dissociation constant (K_d) of the radioligand as determined in saturation binding experiments, and X is the logmolar concentration of unlabelled compound.

4.4. Receptor functional assays

4.4.1. Functional assays at D_2 receptors

The efficacy of compounds at D_2 receptors was investigated in assays of cAMP accumulation in the CHO-K1 cell line stably expressing the cloned human D_{2S} receptor employed in radioligand binding assays. Cellular cAMP levels were quantified by using the homogeneous time-resolved fluorescence (HTRF)-based cAMP kit cAMP-Gs Dynamic HTRF Kit (Cisbio, Bioassays, Codolet, France) following the manufacturer protocol. For initial assessment of a possible agonist effect of the compounds, cells were seeded in 96-well plates in stimulation buffer containing 500 µM 3-isobutyl-1-methylxanthine (IBMX) and were incubated with compound (from 0.1 nM to 100 µM) or dopamine (from 1 nM to 1 mM) as control agonist for 10 min at 37°C. After this time, 10 µM forskolin was added and cAMP

levels were quantified after 5 min incubation. For initial assessment of possible antagonist effect, compounds (0.1 nM - 100 μM) were added to the cells 5 min prior to the addition of the reference agonist dopamine (1 μM) and assays were subsequently carried out as described above. Haloperidol (0.1 nM - 10 μM) was included in these assays as reference antagonist. In all cases, basal cAMP levels were determined in control wells in the absence of compound, agonist and forskolin. Antagonist potency (pK_b, K_b) of the compounds was quantified by Schild analysis [43]. A set of concentration (10 pM - 1 mM)-response curves of the D_2-like receptor full agonist quinpirole were performed in the absence or presence of three different concentrations of the compounds as antagonists, following determination of cAMP levels as described above. The individual curves were fitted to a sigmoidal dose-response model (Hill slope (nH) = 1) using Prism 6 software (GraphPad, San Diego, CA). Dose ratios (DR) were calculated from the individual curves accordingly to the equation $DR = EC_{50}'/EC_{50}$, being EC_{50}' and EC_{50} the fitted EC_{50} value extracted from the agonist curves performed in the presence or absence of compound, respectively. Data were represented in a Schild plot and the pK_b ($-\log K_b$) value was extracted by linear fitting.

4.4.2. Functional assays at 5-HT_{1A} receptors

The efficacy of compounds at 5-HT_{1A} receptors was investigated in assays of cAMP accumulation in the HEK293 cell line stably expressing the cloned human 5-HT_{1A} employed in radioligand binding assays. Cellular cAMP levels were quantified using the cAMP - Gs Dynamic HTRF Kit (Cisbio, Bioassays, Codolet, France) as indicated for functional assays at D_2 receptors. Cells were seeded in 96-well plates in culture medium (Dulbecco's Modified Eagle's Medium-GlutaMAX™-I (Gibco, ThermoFisher Scientific, Madrid, Spain) supplemented with 10% (v/v) dialyzed fetal bovine serum (Sigma Aldrich, Madrid, Spain), 100 U/mL penicillin/0.1 mg/mL streptomycin (Sigma Aldrich, Madrid, Spain), 2 mM L-glutamine (Sigma Aldrich, Madrid, Spain) and 550 μg/ml Geneticin® G418 (Gibco, ThermoFisher

Scientific, Madrid, Spain) and maintained during 24 hours at 37°C in a 5% CO_2 humidified atmosphere. Prior to the assay, cell supernatant was removed and for assessment of possible agonist effect, cells were incubated with the compounds (10 µM, 100 µM) or 5-carboxamidotryptamine (5-CT) as control agonist (from 0.1 nM to 10 µM) in stimulation buffer containing 500 µM IBMX for 10 min at 37°C. After this time, 1 µM forskolin was added and cAMP levels were quantified after 5 min incubation. Basal cAMP levels were determined in control wells in the absence of compound and forskolin.

4.4.3. Functional assays at 5-HT_{2A} receptors

The efficacy of compounds at 5-HT_{2A} receptors was investigated in assays of inositol phosphate (IP) production in the CHO-K1 cell line stably expressing the cloned human 5-HT_{2A} receptor employed in radioligand binding assays. Cellular IP levels were quantified by using the homogeneous time-resolved fluorescence (HTRF)-based inositol monophosphate kit IP-One Gq kit (Cisbio, Bioassays, Codolet, France) following the manufacturer protocol. Cells were seeded in 96-well plates in culture medium (Dulbecco's Modified Eagle's Medium (Gibco, ThermoFisher Scientific, Madrid, Spain) supplemented with 10% (v/v) dialyzed fetal bovine serum (Sigma Aldrich, Madrid, Spain), 100 U/mL penicillin/0.1 mg/mL streptomycin (Sigma Aldrich, Madrid, Spain) and 2 mM L-glutamine (Sigma Aldrich, Madrid, Spain)) and maintained during 24 hours at 37°C in a 5% CO_2 humidified atmosphere. Prior to the assay, cell supernatant was removed and for assessment of possible agonist effect, cells were incubated with the compounds (from 0.1 nM to 100 µM) or serotonin (5-HT) (0.1 nM - 100 µM) as control agonist in stimulation buffer for 20 min at 37°C. After this time, IP levels were quantified. For assessment of possible antagonist effect, compounds (0.1 nM - 100 µM) were added to the cells 10 min prior to the addition of 1 µM 5-HT and assays were subsequently carried out as described above. Risperidone (0.1 nM – 100 µM) was used as control antagonist in these assays. In all cases, basal IP levels were determined in control wells in the absence of compound and

agonist. Antagonist concentration-response curves were fitted to a sigmoidal dose-response (inhibition) model (Hill slope (nH) = 1; best fit in comparison to sigmoidal dose-response (variable slope) model, $P < 0.05$, extra sum-of-squares F test) using Prism 6 software (GraphPad, San Diego, CA) to retrieve pIC_{50} (-log IC_{50}) values. K_b values of the compounds as 5-HT_{2A} antagonists were estimated according to the Leff-Dougall [22] variant of the Cheng-Prusoff equation $K_b = IC_{50}/((2 + ([Ag]/[EC_{50}])^n)^{1/n} - 1)$, where IC_{50} is the concentration of antagonist that inhibits 5-HT response by a 50%; [Ag] is the concentration of 5-HT employed in the assay, [EC_{50}] is the 5-HT EC_{50} value in these assays and n is the Hill slope.

4.5. Molecular modeling

4.5.1. Compound preparation

The compounds **1**-**20** were modelled using LigPrep [44] from Schrödinger suite of software [45]. In order to determine protonation states at the physiological pH Epik [46] module of Schrödinger suite of software was used.

4.5.2. Molecular docking

The compounds **1**-**20** were docked to the X-ray structure of the human dopamine D_2 receptor in the inactive state (PDB ID: 6CM4) [23] and previously reported homology models of the human serotonin 5-HT_{1A} and 5-HT_{2A} receptors [9]. In case of molecular docking to the human dopamine D_2 receptor the grid was generated based on co-crystallized ligand, risperidone. In case of the human serotonin 5-HT_{1A} and 5-HT_{2A} receptors the grids were generated based on the docked chlorprothixene as previously reported [9]. The hydroxylic groups of the following residues were flexible for molecular docking: Ser 193 (5.43), Ser 194 (5.44) and Thr 412 (7.38) for D_2 receptor, Thr196 (5.40), Ser199 (5.43), Thr200 (5.44) for 5-HT_{1A} receptor and Ser159 (3.36), Ser239 (5.44), Ser242 (5.461) for 5-HT_{2A} receptor (numbers in brackets according to the Ballesteros-Weinstein nomenclature [24]) as previously reported

[47]. Standard precision (SP) method of Glide [48] molecular docking module of Schrödinger suite of software was applied. 50 poses were generated for each compound and each receptor. Visualization of results was performed using Schrödinger suite of software and PyMol v. 2.1.1 [49].

4.6. Behavioral studies

4.6.1. Drugs

For *in vivo* studies, d-amphetamine sulphate (5 mg/kg) was dissolved in saline (0.9% NaCl) and injected subcutaneously (s.c.), whereas compound **5** was dissolved in DMSO (its final concentration of 0.1 %) and then diluted with 0.5% aqueous solution of methylcellulose and injected intraperitoneally (i.p.) 60 min before the tests. Drugs were administered at a volume of 10 ml/kg and fresh drug solutions were prepared on each day of experimentation. Control groups received vehicle injections at the same volume *via* i.p. route of administration at the respective time before the tests.

4.6.2. Animals

The experiments were carried out on six week old naive male Swiss mice, weighing 20–30 g. The mice were housed in cages, 5 individuals per cage in an environmentally controlled rooms (ambient temperature 22 ± 1°C; relative humidity 50 - 60%; 12:12 light:dark cycle, lights on at 8:00). Standard laboratory food (LSM, Agropol-Motycz, Poland) and filtered water were available *ad libitum* except for the short time that they were removed from their cages for testing. All the experimental procedures were carried out in the light phase, between 09.00 a.m. and 14.00 p.m, according to the National Institute of Health Guidelines for the Care and Use of Laboratory Animals and to the European Community Directive for the Care and Use of Laboratory of 24 November 1986 (86/609/EEC), and approved by the Local Ethics Committee for Animal Experimentation (License No. 147/2018). All efforts were made to minimize animal

suffering as well as the number of animals used in the study. The experiments were performed by an observer unaware of the treatment administered.

4.6.3. Motor coordination in chimney test

The motor coordination of mice was evaluated using the chimney test. Before the test, the animals were trained in the chimney apparatus (plexiglass tube, 3 cm in inner diameter, 25 cm long) for 3 min, for 3 days. Then, the animals that were able to leave the chimney up to 15 s were subsequently used for the test. In the testing day, motor impairments were assessed by mouse inability to climb up the tube backwards within 30 s. The test was performed 60 min after injection of compound **5** (50 mg/kg; i.p.) (n = 8) or vehicle (i.p.) (n = 8) treatment.

4.6.4. Spontaneous locomotor activity and amphetamine-induced hyperactivity

The locomotor activity of mice was measured using an animal activity meter Opto-Varimex-4 Auto-Track (Columbus Instruments, OH, USA). This automatic device consists of eight transparent cages with a lid, set of four infrared emitters (each emitter has 16 laser beams) and eight detectors monitoring animal movements. To assess the spontaneous activity of mice, the compound **5** (50 mg/kg; i.p.) or vehicle (as a control) were administered 60 min before the test, and to evaluate the influence of tested compound **5** on amphetamine-induced hyperactivity, each mouse received amphetamine (amph, 5 mg/kg, s.c.) 30 min after injection of vehicle or tested compound. Mice were placed individually in the cages, and motility was measured during 30 min by determining the amount of distance travelled in centimeters [cm]. The cages were cleaned up with 10% ethanol after each mouse.

4.6.5. Forced swim test (FST, Porsolt's test) in mice.

The experiment was carried out according to the method of Porsolt et al. [50,51]. Mice were individually placed in a glass cylinder (25 cm high; 10 cm in diameter) containing water maintained at 23 - 25°C, and were left there for 6 min. The total duration of immobility was recorded during the last 4 min of a 6-min test session. A mouse was regarded as immobile when

it remained floating on the water, making only small movements to keep its head above the water. Additionally, time to the first episode of immobility was measured. A decrease in the duration of immobility and increase of time to the first episode of immobility (latency time) is indicative of an antidepressant-like effect.

4.6.6. Passive avoidance task

The passive avoidance (PA) task measures a long-term memory as it was reported by Venault et al. [52]. The PA apparatus consists of two-compartment acrylic box: one illuminated with fluorescent light (8 W) (10 x 13 x 15 cm) and another darkened (25 x 20 x 15 cm), connected by a guillotine door. Entrance of the animal to the darkened box was punished by an electric foot shock (0.15 mA for 2 s). The PA procedure was previously described [53]. In particular, on the first day of experiment [i.e, training (pre-test)], mice were placed individually into the illuminated compartment and allowed to explore this box. After 30 s, the guillotine door was raised to allow the mice to enter the darkened compartment. When each mouse entered to the darkened box, the guillotine door was closed and an electric foot-shock (0.15 mA) of 2 s duration was delivered immediately to the animal *via* grid floor. The latency time for entering the darkened compartment was recorded (TL1). If the mouse failed to enter the darkened box within 300 s, it was placed into this box (the door was closed) and electric foot-shock was delivered to the animal (TL1 value was recorded as 300 s). 24 h later, in the subsequent trial (retention) the same mouse was again placed individually in the illuminated compartment of the PA apparatus. After an adaptation period (30 s) the door between two compartments was raised and the mouse has time (300 s) to reenter the dark compartment (TL2). No foot-shock was applied in this trial. If the animal did not enter to the dark compartment within 300 s, the test was stopped and TL2 was recorded as 300 s [53,54]. The experimental procedure involved examination of the memory consolidation when animals received compound **5** (50 mg/kg; i.p.) or vehicle (control group) after the pre-test.

4.6.7. Statistical analysis

Data were presented as mean ± SEM. To evaluate the locomotor activity changes, the two-way analysis of variance (ANOVA) was used to determine the effects of compound **5** (treatment), pretreatment (control vs. amph) or interaction between these two factors, followed by Bonferroni *post hoc* test to compare each group to the control group. The *t*-test was used to analyze the effect of compound **5** on coordination of mice and depressive-like behavior in the FST, to compare the differences between the studied drug and control group. The confidence limit of $p<0.05$ was considered statistically significant.

For the memory related responses the changes in PA performance were expressed as the difference between retention and training latencies and were taken as a latency index (IL). IL was calculated for each animal and reported as the ratio [8,29]:

IL = TL2−TL1/TL1, where

TL1 – time taken to enter the dark compartment during the training,

TL2 – time taken to reenter the dark compartment during the retention.

Author contributions

Conceptualization, Agnieszka A. Kaczor; Funding acquisition, Agnieszka A. Kaczor, Marián Castro and Maria I. Loza; Investigation, Magda Kondej, Tomasz M. Wróbel, Andrea G. Silva, Piotr Stępnicki, Oliwia Koszła, Ewa Kędzierska, Agata Bartyzel, Marián Castro and Agnieszka A. Kaczor; Methodology, Magda Kondej, Tomasz M. Wróbel, Andrea G. Silva, Piotr Stępnicki, Oliwia Koszła, Ewa Kedzierska, Agata Bartyzel, Marián Castro and Agnieszka A. Kaczor. The manuscript was written through contributions of all authors. All authors have given approval to the final version of the manuscript.

Declaration of interests

The authors declare no conflict of interest.

Acknowledgments

The research was performed under OPUS grant from National Science Center (NCN, Poland), grant number 2017/27/B/NZ7/01767 (to A.A.K). Calculations were partially performed under a computational grant by Interdisciplinary Center for Mathematical and Computational Modeling (ICM), Warsaw, Poland, grant number G30-18 (to A.A.K and D.M.), under resources and licenses from CSC, Finland (to A.A.K). *In vitro* pharmacology assays were performed with support from the Spanish Ministry of Economy and Competitiveness (MINECO) (grant number SAF2014-57138-C2-1-R to M.I.L. and M.C.). A.G.S. acknowledges funding from XUNTA de Galicia (Spain). We thank Rocío Piña Márquez and the USEF screening platform at the University of Santiago de Compostela for their assistance with *in vitro* pharmacological assays.

References

1. Kondej, M.; Stępnicki, P.; Kaczor, A.A. Multi-target approach for drug discovery against schizophrenia. *Int. J. Mol. Sci.* **2018**, *19*, 3105, DOI: 10.3390/ijms19103105.
2. Roth, B.L.; Sheffler, D.J.; Kroeze, W.K. Magic shotguns versus magic bullets: selectively non-selective drugs for mood disorders and schizophrenia. *Nat. Rev. Drug Discov.* **2004**, *3*, 353–359, DOI: 10.1038/nrd1346.
3. GBD 2016 Disease and Injury Incidence and Prevalence Collaborators Global, regional, and national incidence, prevalence, and years lived with disability for 328 diseases and injuries for 195 countries, 1990-2016: a systematic analysis for the Global Burden of Disease Study 2016. *Lancet* **2017**, *390*, 1211–1259, DOI: 10.1016/S0140-6736(17)32154-2.
4. Stępnicki, P.; Kondej, M.; Kaczor, A.A. Current Concepts and Treatments of Schizophrenia. *Molecules* **2018**, *23*, pii: E2087, DOI: 10.3390/molecules23082087.
5. Bakhshi, K.; Chance, S.A. The neuropathology of schizophrenia: A selective review of past studies and emerging themes in brain structure and cytoarchitecture. *Neuroscience* **2015**, *303*, 82–102, oi: 10.1016/j.neuroscience.2015.06.028.

6. Ginovart, N.; Kapur, S. Role of dopamine D(2) receptors for antipsychotic activity. *Handb. Exp. Pharmacol.* **2012**, 27–52, doi: 10.1007/978-3-642-25761-2_2.
7. Lameh, J.; Burstein, E.S.; Taylor, E.; Weiner, D.M.; Vanover, K.E.; Bonhaus, D.W. Pharmacology of N-desmethylclozapine. *Pharmacol. Ther.* **2007**, *115*, 223–231, DOI: 10.1016/j.pharmthera.2007.05.004.
8. Kaczor, A.A.; Silva, A.G.; Loza, M.I.; Kolb, P.; Castro, M.; Poso, A. Structure-Based Virtual Screening for Dopamine D2 Receptor Ligands as Potential Antipsychotics. *ChemMedChem* **2016**, *11*, 718–729, DOI: 10.1002/cmdc.201500599.
9. Kaczor, A.A.; Targowska-Duda, K.M.; Budzyńska, B.; Biała, G.; Silva, A.G.; Castro, M. In vitro, molecular modeling and behavioral studies of 3-{[4-(5-methoxy-1H-indol-3-yl)-1,2,3,6-tetrahydropyridin-1-yl]methyl}-1,2-dihydroquinolin-2-one (D2AAK1) as a potential antipsychotic. *Neurochem. Int.* **2016**, *96*, 84–99, DOI: 10.1016/j.neuint.2016.03.003.
10. Guillaume, J.; Dumont, C.; Laurent, J.; Nédélec, L. (Tétrahydro-1,2,3,6 pyridinyl-4)-3 1H-indoles: synthèse, propriétés sérotoninergique et anti-dopaminergiques. *Eur. J. Med. Chem.* **1987**, *22*, 33–43, DOI: 10.1016/0223-5234(87)90172-3.
11. Freter, K. 3-Cycloalkenylindoles. *J. Org. Chem.* **1975**, *40*, 2525–2529, DOI: 10.1021/jo00905a023.
12. Allen, F. H.; Watson, D. G.; Brammer, L.; Orpen, A. G.; Taylor, R. Chapter 9.5 Typical interatomic distances: organic compounds in International Tables for Crystallography, John Wiley & Sons, Ltd, **2006**.
13. Kondej, M.; Bartyzel, A.; Pitucha, M.; Wróbel, T.M.; Silva, A.G.; Matosiuk, D.; Castro, M.; Kaczor, A.A. Synthesis, Structural and Thermal Studies of 3-(1-Benzyl-1,2,3,6-tetrahydropyridin-4-yl)-5-ethoxy-1H-indole (D2AAK1_3) as Dopamine D_2 Receptor Ligand. *Molecules* **2018**, *23*, pii: E2249. DOI: 10.3390/molecules23092249.

14. Bates, R. B.; Bruck, M. A.; Camou, F. A.; Martin, A. R.; Nikam, S. S.; Nelson, D. L. 3-(1-Methyl-1,2,3,6-tetrahydropyrid-4-yl)indole. *Acta Cryst*. **1989**, *C45*, 109-111, DOI: 10.1107/S0108270188010054.

15. Rasztawicka, M.; Wolska, I.; Maciejewska, D. Solid state structure by X-ray and 13C CP/MAS NMR of new 5,5′-diethoxy-3,3′-methanediyl-bis-indole *J. Mol. Struct.* **2007**, *831*, 174-179, DOI: 10.1016/j.molstruc.2006.08.003.

16. Chandrakantha, T. N.; Puttaraja, P.; Kokila, M. K.; Shivaprakash, N. C. Ethyl 5-Ethoxy-3-methyl-1H-indole-2-carboxylate. *Acta Cryst.* **1998**, *C54*, 1685-1687, DOI: 10.1107/S010827019800568X.

17. Cremer, D.; Pople, J. A. General definition of ring puckering coordinates. *J. Am. Chem. Soc.* **1975**, *97*, 1354-1358, DOI: 10.1021/ja00839a011.

18. Boeyens, J. C. A. The conformation of six-membered rings. *J. Cryst. Mol. Struct*. **1978**, *8*, 317-320, DOI: 10.1007/BF01200485.

19. Pérez, P J.; Carrascosa, R.; García, L.; Barandika, G.; Calderón-Casado, A.; Pérez, E.; Serrano, J. L.; Santana, M. D. Coordination to metal centers: A tool to fix high energy conformations in organic molecules. Application to 2,4,4-trimethyl-1,5,9-triazacyclododec-1-ene and related macrocycles. *Dalton Trans.* **2011**, *40*, 9504–9511, DOI: 10.1039/C1DT11281C.

20. Mayes, H.B.; Broadbelt, L.J.; Beckham, G. T. How sugars pucker: electronic structure calculations map the kinetic landscape of five biologically paramount monosaccharides and their implications for enzymatic catalysis. *J. Am. Chem. Soc.* **2014**, *136*, 1008-1022, DOI: 10.1021/ja410264d.

21. Bernstein, J.; Davis, R.E.; Shimoni, L.; Chang, N.-L. Patterns in hydrogen bonding: functionality and graph set analysis in crystals, *Angew. Chem. Int. Ed. Engl.*, **1995**, *34,* 1555–1573, DOI: 10.1002/anie.199515551.

22. Leff, P.; Dougall, I.G. Further concerns over Cheng-Prusoff analysis. *Trends Pharmacol. Sci.* **1993**, *14*, 110–112, DOI: 10.1016/0165-6147(93)90080-4.

23. Wang, S.; Che, T.; Levit, A.; Shoichet, B.K.; Wacker, D.; Roth, B.L. Structure of the D_2 dopamine receptor bound to the atypical antipsychotic drug risperidone. *Nature* **2018**, *555*, 269–273, DOI: 10.1038/nature25758.

24. Ballesteros, J. A.; Weinstein, H. Integrated methods for the construction of three-dimensional models and computational probing of structure-function relations in G protein-coupled receptors. *Methods in neurosciences* **1995**, *25*, 366–428, DOI: 10.1016/S1043-9471(05)80049-7.

25. Selent, J.; Marti-Solano, M.; Rodríguez, J.; Atanes, P.; Brea, J.; Castro, M.; Sanz, F.; Loza, M.I.; Pastor, M. Novel insights on the structural determinants of clozapine and olanzapine multi-target binding profiles. *Eur. J. Med. Chem.* **2014**, *77*, 91–95, DOI: 10.1016/j.ejmech.2014.02.058.

26. Zhang, G.; Stackman, R.W. The role of serotonin 5-HT2A receptors in memory and cognition. *Front. Pharmacol.* **2015**, *6*, 225, DOI: 10.3389/fphar.2015.00225.

27. Leucht, S.; Cipriani, A.; Spineli, L.; Mavridis, D.; Orey, D.; Richter, F.; Samara, M.; Barbui, C.; Engel, R.R.; Geddes, J.R.; Kissling, W.; Stapf, M.P.; Lässig, B.; Salanti, G.; Davis, J. M. Comparative efficacy and tolerability of 15 antipsychotic drugs in schizophrenia: a multiple-treatments meta-analysis. *Lancet* **2013**, *382*, 951–962, DOI: 10.1016/S0140-6736(13)60733-3.

28. McCreary, A.C.; Newman-Tancredi, A. Serotonin 5-HT1A receptors and antipsychotics - an update in light of new concepts and drugs. *Curr. Pharm. Des.* **2015**, *21*, 3725–3731, DOI: 10.2174/1381612821666150605105215.

29. Bartels, B.; Weinbrenner, S.; Marx, D.; Diefenbach, J.; Dunkern, T.; Menge, W. M. P. B.; Christiaans, J. A. M. Benzyl-substituted tetracyclic heterocyclic compounds. PCT Int. Appl., 2010015588, **2010**.

30. Klaveness, J.; Brudeli, B.; Levy, F. O. 5-htx modulators. PCT Int. Appl., 2007007072, **2007**.

31. Xue, S.; Hao, Z.; Sun, C. Preparation of N-substituted tetrahydropyridyl indole compounds as antitumor agents. Faming Zhuanli Shenqing, CN 102276581 A 20111214, **2011**.

32. Agarwal, A.; Pearson, P.P.; Taylor, E.W.; Li, H.B.; Dahlgren, T.; Herslöf, M.; Yang, Y.; Lambert, G.; Nelson, D.L.; Regan, J.W. Three-dimensional quantitative structure-activity relationships of 5-HT receptor binding data for tetrahydropyridinylindole derivatives: a comparison of the Hansch and CoMFA methods. *J. Med. Chem.* **1993**, *36*, 4006–4014, DOI: 10.1021/jm00077a003.

33. Sun, C.; Xiao, D.; Li, J.; Xue, S.; Li, X. Preparation of N-substituted tetrahydropyridinyl indole-conjugated anti-CD14 monoclonal antibody for treatment of leukemia. Faming Zhuanli Shenqing, CN 102898523 A 20130130, **2013**.

34. Gharagozloo, P.; Miyauchi, M.; Birdsall, N.J.M. 3-(Tetrahydropyridinyl)indoles. *Tetrahedron* **1996**, *52*, 10185–10192, DOI: 10.1016/0040-4020(96)00553-4.

35. CrysAlis PRO, ed. Yarnton, Oxfordshire, UK Agilent Technologies Ltd., **2013.**

36. Sheldrick, G. M. A short history of SHELX. *Acta Cryst.* **2008**, *A64*, 112-122, DOI: 10.1107/S0108767307043930.

37. Faruggia, L.J. WinGX suite for small-molecule single-crystal crystallography. *J. Appl. Crystallogr.* **1999**, *32*, 837-838, DOI: 10.1107/S0021889899006020.

38. Spek, L. A. Single-crystal structure validation with the program PLATON. J. Appl. Cryst. **2003**, *36*, 7-13, DOI: 10.1107/S0021889802022112.

39. Farrugia, L. J. WinGX and ORTEP for Windows: an update. *J. Appl. Cryst.* **2012**, *45*, 849-854, DOI: 10.1107/S0021889812029111.
40. Macrae, C.F.; Edgington, P.R.; McCabe, P.; Pidcock, E.; Shields, G.P.; Taylor, R.; Towler, M.; van de Streek, J. Mercury: Visualization and Analysis of Crystal Structures. *J. Appl. Cryst.* **2006**, *39*, 453-457, DOI: 10.1107/S002188980600731X.
41. Brea, J.; Rodrigo, J.; Carrieri, A.; Sanz, F.; Cadavid, M.I.; Enguix, M.J.; Villazón, M.; Mengod, G.; Caro, Y.; Masaguer, C.F.; Raviña, E.; Centeno, N. B.; Carotti, A.; Loza, M. I. New serotonin 5-HT(2A), 5-HT(2B), and 5-HT(2C) receptor antagonists: synthesis, pharmacology, 3D-QSAR, and molecular modeling of (aminoalkyl)benzo and heterocycloalkanones. *J. Med. Chem.* **2002**, *45*, 54–71, DOI: 10.1021/jm011014y.
42. Kucwaj-Brysz, K.; Warszycki, D.; Podlewska, S.; Witek, J.; Witek, K.; González Izquierdo, A.; Satała, G.; Loza, M.I.; Lubelska, A.; Latacz, G.; Bojarski, A. J.; Castro, M.; Kieć-Kononowicz, K.; Handzlik, J. Rational design in search for 5-phenylhydantoin selective 5-HT7R antagonists. Molecular modeling, synthesis and biological evaluation. *Eur. J. Med. Chem.* **2016**, *112*, 258–269, DOI: 10.1016/j.ejmech.2016.02.024.
43. Kenakin, Terry P.. A Pharmacology Primer: Techniques for More Effective and Strategic Drug Discovery. Fourth Ed. San Diego, CA: Academic Press, **2014**.
44. Schrödinger Release 2019-2: LigPrep, Schrödinger, LLC, New York, NY, **2019**.
45. Small-Molecule Drug Discovery Suite 2019-2, Schrödinger, LLC, New York, NY, **2019**.
46. Schrödinger Release 2019-2: Epik, Schrödinger, LLC, New York, NY, **2019**.
47. Magli, E.; Kędzierska, E.; Kaczor, A.A.; Severino, B.; Corvino, A.; Perissutti, E.; Frecentese, F.; Saccone, I.; Massarelli, P.; Gibuła-Tarłowska, E.; Kotlińska, J. H.; Santagada, V.; Caliendo, G.; Fiorino, F. Synthesis, docking studies, and pharmacological evaluation of 5-HT_{2C} ligands containing the N'-cyanoisonicotinamidine or N'-

cyanopicolinamidine nucleus. *Arch. Pharm. (Weinheim)* **2019**, *352*, e1800373, DOI: 10.1002/ardp.201800373.

48. Schrödinger Release 2019-2: Glide, Schrödinger, LLC, New York, NY, **2019**.
49. The PyMOL Molecular Graphics System, Version 2.1.1 Schrödinger, LLC.
50. Porsolt, R.D.; Bertin, A.; Jalfre, M. Behavioral despair in mice: a primary screening test for antidepressants. *Arch. Int. Pharmacodyn. Ther.* **1977**, *229*, 327–336.
51. Porsolt, R.D.; Le Pichon, M.; Jalfre, M. Depression: a new animal model sensitive to antidepressant treatments. *Nature* **1977**, *266*, 730–732.
52. Venault, P.; Chapouthier, G.; de Carvalho, L.P.; Simiand, J.; Morre, M.; Dodd, R.H.; Rossier, J. Benzodiazepine impairs and beta-carboline enhances performance in learning and memory tasks. *Nature* **1986**, *321*, 864–866, DOI: 10.1038/321864a0.
53. Budzynska, B.; Boguszewska-Czubara, A.; Kruk-Slomka, M.; Skalicka-Wozniak, K.; Michalak, A.; Musik, I.; Biala, G.; Glowniak, K. Effects of imperatorin on nicotine-induced anxiety- and memory-related responses and oxidative stress in mice. *Physiol. Behav.* **2013**, *122*, 46–55, DOI: 10.1016/j.physbeh.2013.08.019.
54. Allami, N.; Javadi-Paydar, M.; Rayatnia, F.; Sehhat, K.; Rahimian, R.; Norouzi, A.; Dehpour, A.R. Suppression of nitric oxide synthesis by L-NAME reverses the beneficial effects of pioglitazone on scopolamine-induced memory impairment in mice. *Eur. J. Pharmacol.* **2011**, *650*, 240–248, DOI: 10.1016/j.ejphar.2010.10.007.
55. Hogle, J.M.; Kaye, J.T.; Curtin, J.J. Nicotine withdrawal increases threat-induced anxiety but not fear: neuroadaptation in human addiction. *Biol. Psychiatry* **2010**, *68*, 719–725, DOI: 10.1016/j.biopsych.2010.06.003.